Atmos. Meas. Tech., 14, 3953–3972, 2021
https://doi.org/10.5194/amt-14-3953-2021
© Author(s) 2021. This work is distributed under
the Creative Commons Attribution 4.0 License.

Atmospheric Measurement Techniques
Open Access
EGU

Systematic comparison of vectorial spherical radiative transfer models in limb scattering geometry

Daniel Zawada[1], Ghislain Franssens[2], Robert Loughman[3], Antti Mikkonen[4], Alexei Rozanov[5], Claudia Emde[6], Adam Bourassa[1], Seth Dueck[1], Hannakaisa Lindqvist[4], Didier Ramon[7], Vladimir Rozanov[5], Emmanuel Dekemper[2], Erkki Kyrölä[4], John P. Burrows[5], Didier Fussen[2], and Doug Degenstein[1]

[1]Institute of Space and Atmospheric Studies, University of Saskatchewan, Saskatchewan, Canada
[2]Royal Belgian Institute for Space Aeronomy, Brussels, Belgium
[3]Department of Atmospheric and Planetary Sciences, Hampton University, Hampton, Virginia, USA
[4]Finnish Meteorological Institute, Helsinki, Finland
[5]Institute of Environmental Physics, University of Bremen, Bremen, Germany
[6]Meteorological Institute, Ludwig-Maximilians-Universität, Munich, Germany
[7]HYGEOS, Lille, France

Correspondence: Daniel Zawada (daniel.zawada@usask.ca)

Received: 27 November 2020 – Discussion started: 4 January 2021
Revised: 16 April 2021 – Accepted: 19 April 2021 – Published: 28 May 2021

Abstract. A comprehensive inter-comparison of seven radiative transfer models in the limb scattering geometry has been performed. Every model is capable of accounting for polarization within a spherical atmosphere. Three models (GSLS, SASKTRAN-HR, and SCIATRAN) are deterministic, and four models (MYSTIC, SASKTRAN-MC, Siro, and SMART-G) are statistical using the Monte Carlo technique. A wide variety of test cases encompassing different atmospheric conditions, solar geometries, wavelengths, tangent altitudes, and Lambertian surface reflectances have been defined and executed for every model. For the majority of conditions it was found that the models agree to better than 0.2 % in the single-scatter test cases and better than 1 % in the scalar and vectorial test cases with multiple scattering included, with some larger differences noted at high values of surface reflectance. For the first time in limb geometry, the effect of atmospheric refraction was compared among four models that support it (GSLS, SASKTRAN-HR, SCIATRAN, and SMART-G). Differences among most models with multiple scattering and refraction enabled were less than 1 %, with larger differences observed for some models. Overall the agreement among the models with and without refraction is better than has been previously reported in both scalar and vectorial modes.

1 Introduction

The limb scattering measurement technique involves viewing through the side, the limb, of the atmosphere while measuring scattered sunlight (see Fig. 1). Measurements are performed in the ultraviolet, visible, and near-infrared spectral ranges where scattering of solar irradiance is the dominant source of measured radiation. Scattering occurs through Rayleigh scattering from the background atmosphere, as well as potential contributions of scattering from larger particles such as stratospheric aerosols and clouds. The signal is also affected through absorption by atmospheric constituents, typically by molecules such as ozone or nitrogen dioxide in the ultraviolet and visible. In the near and shortwave infrared, absorption is dominated by water vapor, methane, carbon dioxide, and molecular oxygen.

Several satellite-based limb scattering instruments have flown in the past few decades. Notably, the Optical Spectrograph and InfraRed Imager System (OSIRIS; Llewellyn et al., 2004) was launched on board the Swedish satellite Odin (Murtagh et al., 2002) in 2001, the SCanning Imaging Absorption SpectroMeter for Atmospheric CHartographY (SCIAMACHY; Bovensmann, 1999) instrument on board Envisat in 2002, and the Ozone Mapping and Profiler Suite Limb Profiler (OMPS-LP; Flynn et al., 2006) on

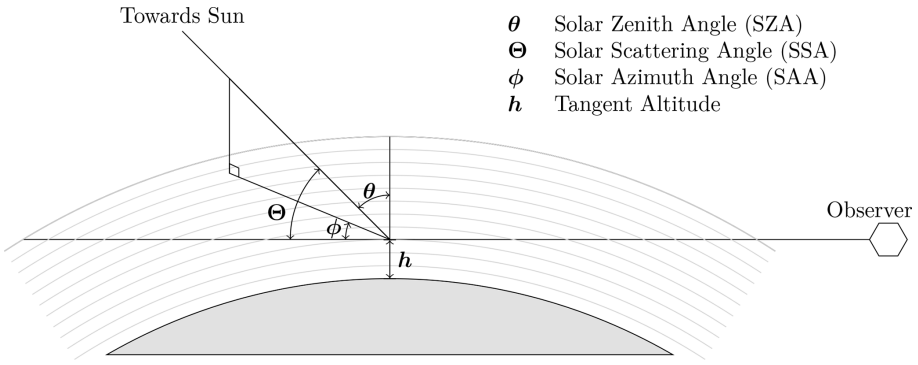

Figure 1. The limb-viewing geometry and definitions of solar zenith angle, solar azimuth angle, solar scattering angle, and tangent altitude. The tangent altitude and solar zenith angles are defined relative to the un-refracted tangent point such that a solar scattering angle of 0° is perfect forward scatter, and a solar zenith angle of 0° is the sun directly overhead. Figure adapted from Zawada et al. (2015).

board Suomi-NPP in 2011. Two versions of the primarily solar occultation instrument the Stratospheric Aerosol and Gas Experiment (SAGE), SAGE III-M (Mauldin et al., 1998) on Meteor-3M in 2001, and SAGE III-ISS (Cisewski et al., 2014) on the International Space Station (ISS) in 2016 have the capability to make limb scatter measurements. The stellar occultation instrument, Global Ozone Monitoring by Occultation of Stars (GOMOS; Kyrölä et al., 2004), is also capable of taking limb scatter measurements. OMPS-LP is planned to be re-launched on board the JPSS-2 satellite in 2022, and a new instrument, the Atmospheric Limb Tracker for Investigation of the Upcoming Stratosphere (ALTIUS; Fussen et al., 2019), is currently under development by the European Space Agency for a planned 2024 launch.

Vertical profiles of limb scattering spectra can be inverted to obtain distributions of atmospheric constituents with spectral absorption or scattering features. These include but are not limited to stratospheric aerosol (Bourassa et al., 2007; von Savigny et al., 2015), ozone (Roth et al., 2007; Degenstein et al., 2009; Rault and Spurr, 2010; Arosio et al., 2018), nitrogen dioxide (Butz et al., 2006; Sioris et al., 2017), water vapor (Rozanov et al., 2011b), and bromine oxide (McLinden et al., 2010; Rozanov et al., 2011a). Inversion of these spectra require a radiative transfer model (RTM) capable of simulating the observed radiance, including all relevant physical effects for the constituent of interest. The accuracy of the RTM directly influences the accuracy of the retrieved profile.

All of the aforementioned retrieval methods use RTMs operating in scalar mode, where only the intensity, I, is computed rather than the full Stokes vector of the observed radiance. This is known to be a good approximation when the instrument itself is designed to be polarization insensitive. While there do exist errors in the intensity from neglecting polarization (Mishchenko et al., 1994), they tend to cancel in various normalization schemes used by the retrieval (Loughman et al., 2005). However, ALTIUS and similar instrument concepts (Elash et al., 2017; Kozun et al., 2020) are designed to measure a linear polarized signal rather than the raw intensity. For these instruments it is required to use an RTM that is capable of simulating the full Stokes vector.

Several studies have been performed which inter-compare the accuracy of polarized RTMs (e.g., Emde et al., 2015, 2018); however these have been focused on viewing angles of, at most, 80° (a viewing angle of 90° would be limb viewing). For viewing geometries other than limb and occultation, it is common to use the plane-parallel assumption, which is generally not applicable in the limb geometry. The approximate spherical approach, where single-scattered radiance is calculated using a spherical atmosphere and the multiple-scatter signal is approximated with a plane-parallel model, has been shown to have systematic errors in the limb-viewing geometry (Loughman et al., 2004; McLinden and Bourassa, 2010). Recently, Korkin et al. (2020) have extended some of these results to a fully spherical atmosphere, but the scope of the project was limited to scalar radiative transfer.

The most comprehensive previous inter-comparison focusing on the limb scattering geometry was performed by Loughman et al. (2004). The deterministic models Gauss–Seidel limb scattering (GSLS), CDI, and CDIPI (Rozanov et al., 2001, which are solvers implemented in SCIATRAN), and the statistical models Siro (Oikarinen et al., 1999) and MCC++ (Postylyakov, 2004) were considered. It was found that the statistical models generally agree to within 1.5 % with multiple scattering enabled, while the deterministic spherical models, CDIPI and GSLS, agree with the statistical models at the 2 %–4 % level. While comparison of the full Stokes vector was included for models that supported it, it was not the primary goal of the study. The results of this study have been used in benchmarking newly developed RTMs, such as SASKTRAN (Bourassa et al., 2008), or to evaluate new updates or features of RTMs as was done for GSLS (Loughman et al., 2015).

This study serves to both update the state of inter-comparison of RTMs in limb scattering geometry and to improve on it in several ways. Firstly, all participating RTMs

simulate polarization in the atmosphere and provide full Stokes vectors which are compared; these results are of significant importance for the upcoming ALTIUS mission. Secondly, the treatment of stratospheric aerosols is updated to use Mie scattering solution rather than a Henyey–Greenstein phase function; the Mie scattering treatment is more representative of the current state of limb retrievals (e.g., Rieger et al., 2019; Malinina et al., 2019; Taha et al., 2021). In addition, simulations including atmospheric refraction are included for the first time. All of the model results are made publicly available to be used as a benchmark in future studies in Zawada et al. (2020).

Descriptions of each model are presented in Sect. 2, with Sect. 3 describing the setup of the test cases in detail. The results and discussion of the comparisons can be found in Sect. 4 with final conclusions in Sect. 5.

2 Model descriptions

Generally, modern RTMs include a variety of tools to aid in specifying the atmospheric state and the viewing geometry. These could be relatively simple things such as precomputed climatologies of pressure, temperature, and ozone, or something more involved such as a built-in Mie scattering code to calculate the optical properties of stratospheric aerosol particles of a given size distribution. However, the core purpose of every RTM is to solve the radiative transfer equation. Some models may contain several algorithms to do this, and each one is called a *solver* or *engine*. In many cases, these solvers start from fundamentally different assumptions and have their own characteristic features. For example, the RTM SCIATRAN contains several solvers; however only one (Discrete Ordinates Method-Vector) is capable of simulating polarized radiances (Stokes vectors). Two polarized engines are included in this study for SASKTRAN, SASKTRAN-HR and SASKTRAN-MC, which solve the radiative transfer problem in a successive order and with the Monte Carlo (MC) methods, respectively.

RTMs typically belong to one of two classes: statistical or deterministic. Statistical models solve the radiative transfer equation using Monte Carlo simulation of photon paths through the atmosphere, while deterministic models use discretization, interpolation, and various simplifying assumptions. Statistical models are often easier to implement since fewer assumptions are made; however they usually are orders of magnitude slower computationally.

2.1 Deterministic models

Deterministic models solve the radiative transfer equation (RTE) using some form of numerical integration over the line of sight (LOS) and by making various simplifying assumptions. The choice of how and which quantities are discretized can result in completely different methods being applied to solving the RTE.

These methods can further be classified according to how the sphericity of the atmosphere is handled when calculating the multiple-scattered radiance field. Plane-parallel models assume a flat Earth and can therefore not be applied to simulate the limb-viewing geometry. Pseudo-spherical models employ a plane-parallel solution but initialize the data in the RTE with the solar irradiance attenuated through a spherical atmosphere. Approximate spherical models trace the observer LOS through a spherical atmosphere, calculate the single-scatter term spherically, and then use an approximately spherical multiple-scatter source function for light that has been scattered more than once (typically from one or more pseudo-spherical calculations, although the exact method may vary from model to model). Lastly, fully spherical models account for sphericity in all aspects of the calculation.

Some of these approximations have been shown to have significant systematic effects on calculated radiances in the limb-viewing geometry. Most notably, approximate spherical methods which use a single plane-parallel solution for the multiple-scatter source have been shown to be systematically high (on the order of 5 %) at higher tangent altitudes (McLinden and Bourassa, 2010). Similar differences were noted by Loughman et al. (2004) in comparing approximate spherical models with fully spherical statistical models.

2.1.1 GSLS

The Gauss–Seidel limb scattering (GSLS) RTM builds upon the techniques described by Herman et al. (1994, 1995) to simulate the vectorial radiance in a spherical atmosphere. Line-of-sight rays are traced through a fully spherical atmosphere, integrating a fully spherical single-scatter source function and an approximate multiple-scatter source. The approximate multiple-scatter source is calculated at a selected number of solar zenith angles using a pseudo-spherical calculation. The number of solar zenith angles at which the multiple-scatter source function is calculated at depends on the solar geometry and is shown in Loughman et al. (2015). GSLS has support for atmospheric refraction and analytic computation of approximate weighting functions. A full description of GSLS can be found within Loughman et al. (2004, 2015).

GSLS has been used in several projects involving the retrieval of atmospheric constituents from limb scatter measurements. Most notably, GSLS is currently used as the RTM for the operational version of the OMPS-LP ozone and stratospheric aerosol data products (Rault and Loughman, 2013). The OMPS-LP stratospheric aerosol algorithm has also been applied to SCIAMACHY measurements (Taha et al., 2011). GSLS was also used in experimental retrievals using limb scatter measurements from SAGE III-M (Rault, 2005).

2.1.2 SASKTRAN-HR

SASKTRAN is a fully spherical, vectorial RTM originally developed at the University of Saskatchewan to process data from the Optical Spectrograph and InfraRed Imaging System (OSIRIS; Llewellyn et al., 2004) instrument. A full description of SASKTRAN can be found in Bourassa et al. (2008) and Zawada et al. (2015), and details on the polarized calculation can be found in Dueck et al. (2017) and can be found online at https://arg.usask.ca/docs/sasktran/ (last access: 16 April 2021). SASKTRAN includes both a statistical (SASKTRAN-MC; see Sect. 2.2.2) and a deterministic method (SASKTRAN-HR) to solve the RTE. The deterministic approach employs the successive order of scattering technique. The technique has a physical interpretation where radiance incident from the sun directly is used to calculate the single-scattered radiance. The single-scatter radiance is then used to calculate the second order of scatter, and the process is iterated until convergence. Refractive effects can also optionally be included, approximate analytic weighting functions can be calculated, and two- and three-dimensional atmospheres can be handled. The primary application of SASKTRAN has been as the forward model for retrievals of ozone (Degenstein et al., 2009), stratospheric aerosols (Bourassa et al., 2007), and nitrogen dioxide (Sioris et al., 2017) from the OSIRIS instrument. However, SASKTRAN has also been used in a variety of projects unrelated to OSIRIS. SASKTRAN has been adapted to process limb retrievals from other instruments, including stratospheric aerosols from SCIAMACHY measurements (Rieger et al., 2018) and stratospheric ozone from OMPS-LP measurements (Zawada et al., 2018). SASKTRAN was also used to analyze data from an acousto-optical tuneable filter-based instrument, the Aerosol Limb Imager (ALI; Elash et al., 2016), which is conceptually similar to the vis–NIR channel of ALTIUS.

SASKTRAN-HR has various options that control the accuracy of the solution, but the main one is the number of diffuse profiles, i.e., the number of discretizations used in solar zenith angle to compute the multiple-scatter field. The model has been configured to use the number of diffuse profiles required to obtain approximately 0.2 % accuracy as a function of solar conditions shown in Zawada et al. (2015).

2.1.3 SCIATRAN

The SCIATRAN software package provides tools for modeling radiative transfer processes in the ultraviolet to thermal infrared spectral range. A detailed review of available algorithms, selected comparisons, and applications is given by Rozanov et al. (2014), and more information can be found at https://www.iup.uni-bremen.de/sciatran/ (last access: 16 April 2021). SCIATRAN contains databases (or code modules) of optical properties and climatologies and a set of engines to solve the RTE. The only solver capable of simulating the vectorial radiance field is the discrete ordinates method – vector (DOM-V) solver. The DOM-V solver uses the discrete ordinates method to simulate the pseudo-spherical solution used to initialize the spherical integration.

In the limb-viewing geometry SCIATRAN can operate in two modes, fully spherical and approximately spherical. In the approximately spherical mode, the single-scatter radiance is calculated accounting for the full sphericity of the Earth, while the multiple-scattered signal is approximated by several pseudo-spherical calculations. In fully spherical mode, the approximately spherical solution is iterated in a fully spherical geometry to account for sphericity effects. SCIATRAN uses the fully spherical mode in the shown comparisons.

SCIATRAN accounts for refractive effects and calculates approximate weighting functions. SCIATRAN has been used in numerous applications spanning multiple research areas. One of SCIATRAN's primary applications is its use as the forward model for SCIAMACHY limb scatter retrievals of including, but not limited to, ozone (Rozanov et al., 2007), water vapor (Rozanov et al., 2011b), and stratospheric aerosols (von Savigny et al., 2015; Malinina et al., 2018). SCIATRAN has also been successfully used in the inversion of data products from the observations of other limb missions, including the retrievals of stratospheric aerosol from OSIRIS measurements (Rieger et al., 2018) and ozone and stratospheric aerosol from OMPS-LP measurements (Arosio et al., 2018; Malinina et al., 2020).

2.2 Statistical models

Statistical models use Monte Carlo (MC) simulation to solve the RTE. In spherical geometry, the most common technique is the so-called backward MC method, or adjoint method. Here, photons are traced, starting at the sensor, through the atmosphere and towards the sun; this is in contrast to the forward method, where photons originate at the source (Sun). Along the photon path, the choice of where the photon scatters and the direction of scattering are sampled based on the probability of a scatter event occurring. The final radiance, and associated precision, are estimated by analyzing an ensemble of a large number of photons. All of the models within this study use a variant of the backward MC method.

The MC technique naturally has few assumptions, which allows for easier implementation of new features. A primary example of this is implementing atmospheric constituents that vary in three dimensions, rather than only in altitude. It is also quite natural to handle the full sphericity of the atmosphere. Because of these reasons, statistical models are primarily used as benchmark models and to study new effects. Statistical models are typically orders of magnitude slower than deterministic models and are thus usually not used in operational retrieval methods. They also contain inherent random noise, driven by the number of photons used

in the simulation, which may need to be considered depending on the application.

2.2.1 MYSTIC

The Monte carlo code for the phYSically correct Tracing of photons In Cloudy atmospheres (MYSTIC) model (Mayer, 2009; Emde et al., 2010) is a statistical, fully spherical, polarized RTM that is distributed as part of the libRadtran software package (Emde et al., 2016; Mayer and Kylling, 2005), which is available online (http://www.libradtran.org/, last access: 16 April 2021). Mystic is capable of simulating radiances, irradiances, heating rates, and actinic fluxes in the solar and thermal spectral ranges. While MYSTIC was originally designed for applications in three-dimensional cloudy atmospheres, it contains the full functionality necessary to simulate limb-scattered radiances. In spherical mode, MYSTIC uses the backward MC method. MYSTIC contains specialized variance reduction methods for handling strongly peaked phase functions (Buras and Mayer, 2011) and is capable of handling atmospheres where the parameters vary in three dimensions (not just in altitude) (Emde and Mayer, 2007; Emde et al., 2017). High-spectral-resolution radiances can be simulated efficiently using the ALIS (Absorption Lines Importance Sampling) method (Emde et al., 2011).

2.2.2 SASKTRAN-MC

The SASKTRAN RTM contains a MC mode (SASKTRAN-MC) based upon the Siro algorithm (Oikarinen et al., 1999). The primary purpose of SASKTRAN-MC is to serve as a benchmark for the SASKTRAN-HR model. SASKTRAN-MC is fully polarized, spherical, and also uses the backward MC method. SASKTRAN-MC is capable of handling three-dimensional atmospheres and includes options to simulate the radiance to a specific precision level, rather than specifying the absolute number of photons to simulate. For more details, see Zawada et al. (2015), Dueck et al. (2017), and https://arg.usask.ca/docs/sasktran/ (last access: 16 April 2021).

2.2.3 Siro

Siro is a statistical, fully spherical, polarized RTM developed at the Finnish Meteorological Institute, using the backward MC method (Oikarinen et al., 1999); more information can be found online at http://ikaweb.fmi.fi/ika_models.html#siro (last access: 16 April 2021). Siro is capable of simulating radiances where the atmosphere varies three-dimensionally (not only in altitude). Siro is commonly used as a reference model for both studying limb-scattered radiance and in comparisons with other RTMs. Oikarinen et al. (1999) used Siro to demonstrate the importance of multiple scattering for limb scatter instruments and to simulate the effects of a two-dimensionally varying reflective surface (Oikarinen, 2002). In Oikarinen (2001) the effect of polarization on limb scatter radiance was assessed in detail using Siro. Siro played a key role in the RTM inter-comparison study performed by Loughman et al. (2004) as one of the MC reference models.

2.2.4 SMART-G

SMART-G (Speed-up Monte-carlo Advanced Radiative Transfer code with GPU) is a radiative transfer solver for the coupled ocean–atmosphere system with a wavy interface (Ramon et al., 2019) or any surface spectral bidirectional reflectance distribution function (BRDF) boundary condition. It is based on the MC technique, works in either plane-parallel or spherical-shell geometry, and accounts for polarization. The vectorial code is written in CUDA (Compute Unified Device Architecture) and runs on GPUs (graphics processing units). Physical processes included in the current version of the code are elastic scattering, absorption, reflection, thermal emission, and refraction.

The radiances at any level of the domain can be estimated using the local estimate variance reduction method (Marchuk et al., 2013). Benchmark values are accurately reproduced for clear (Natraj and Hovenier, 2012) and cloudy atmospheres (Kokhanovsky et al., 2010) over a wavy reflecting surface and a black ocean (Emde et al., 2015). For pure Rayleigh atmospheres as in ocean–surface–atmosphere system comparisons, the agreement is better than 1E-5 in intensity and 0.1 % in degree of polarization (Ramon et al., 2019; Chowdhary et al., 2020). The SMART-G code is capable of handling horizontal inhomogeneities of the albedo like adjacency effects (Chowdhary et al., 2019) or three-dimensional variations in the oceanic and atmospheric optical properties.

2.2.5 Differences in the backwards Monte Carlo methods

There is a subtle difference in the way the backwards Monte Carlo method is implemented that can be noticed in the subsequent comparisons. One option is to trace rays through the atmosphere and calculate the scattering probability at each layer interface. This gives the possibility of photons not scattering and directly escaping the atmosphere, which is important for estimates of radiative fluxes (not directly applicable for limb scatter measurements). A consequence of this is that at longer wavelengths and higher tangent altitudes where the atmosphere is optically thin, a large number of photons are required to reduce the statistical noise to acceptable levels. In this study this technique is used by MYSTIC and SMART-G.

An alternative technique is to force every photon traced backwards from the observer to scatter. Random numbers are generated to determine the scatter location, not if scattering actually occurs. Photons can then be weighted by the optical thickness to account for the probability of scattering. A benefit of this technique is that the number of photons required to hit a desired noise floor is more uniform in wavelength and altitude space, but the technique is more specific to limb scattering measurements. Siro and SASKTRAN-MC

both use the same technique where every photon traced is forced to scatter.

SMART-G includes an option to force additional scattering in limb mode, but only for the first (single) scatter. The option has a similar effect to the technique used by Siro/SASKTRAN-MC in that it reduces the variance of the calculation for optically thin scenarios, but it is not exactly equivalent.

Overall, all of the mentioned techniques solve the radiative transfer equation with the same level of accuracy. The only difference is the number of photons required to reach a desired level of precision. A more in-depth discussion of the computational efficiency of the different techniques for different scenarios is presented in Sect. 4.5.

3 Model test cases

Test cases are designed to explore the aspects of the RTMs that are applicable for past, present, and future satellite-based limb-scattering measurements. All tests are performed for the following range of tangent altitudes, solar angles, surface reflectance, atmospheric constituent conditions, and wavelengths:

- 80 tangent altitudes from 0.5 to 79.5 km (inclusive) with a spacing of 1 km.
- 9 combinations of SZA and SAA which are given in Table 1 and are typical for a near-polar sun-synchronous orbit with an equatorial crossing time near noon such as what is planned for ALTIUS.
- 3 values of a Lambertian effective reflectance of 0, 0.3, and 1.
- 3 atmospheric constituent conditions: pure Rayleigh scattering, Rayleigh scattering and ozone absorption, and Rayleigh + stratospheric aerosol scattering and ozone absorption.
- 11 wavelengths provided in Table 2.

These test cases span the reasonable conditions that have been, or are currently, in use by operational limb scatter instruments for retrievals of typical atmospheric constituents.

In addition to different atmospheric and geometry conditions, test cases are selected using different RTM settings:

- single scattering only, vectorial, no refraction;
- multiple scattering included, scalar, no refraction;
- multiple scattering included, vectorial, refraction.

Note that a single-scattering scalar test case would be redundant as the single scatter I is unaffected by polarization when the incident source is unpolarized. In all cases the SZA and SAA are defined at the tangent point of each individual line of sight. The placement of the tangent point assumes straight-line, un-refracted rays, from the observer.

Table 1. Solar zenith angles, solar azimuth angles, and solar scattering angles used in the test cases.

Solar zenith angle	Solar azimuth angle	Solar scattering angle
10°	20°	80.6°
15°	70°	84.9°
35°	90°	90.0°
45°	50°	63.0°
50°	130°	119.5°
60°	70°	72.8°
70°	30°	35.5°
80°	60°	60.5°
80°	150°	148.5°

One of the challenges in performing an inter-comparison of RTMs is ensuring that the inputs are the same across every model. In this study, care was taken so that the input parameters were specified in a way that can be assimilated by every model in the study. Stratospheric aerosol is specified as a log-normal distribution of Mie scattering particles with a median radius of 80 nm and a mode width of 1.6, with scattering parameters (cross sections, Mueller matrices, and Legendre moments) calculated using the code of Wiscombe (1980) and tabulated in wavelength. The refractive index is consistent with that of sulfuric acid and is taken from Palmer and Williams (1975). The ozone absorption cross section is taken from measurements by Brion et al. (1993), Daumont et al. (1992), and Malicet et al. (1995) interpolated to 243 K. Rayleigh scattering is assumed to be elastic and without anisotropy corrections. These parameters are provided for reference in Table 2.

The background atmosphere is specified on a 1 km grid from 0 to 100 km. The ozone profile is taken from a climatology derived from measurements from the Microwave Limb Sounder (Waters et al., 2006) and the Atmospheric Chemistry Experiment (Bernath et al., 2005). Rayleigh scattering number density, pressure, and temperature are taken from typical tropical conditions in the MSIS-E-90 atmospheric model. The GLobal Space-based Stratospheric Aerosol Climatology (GLoSSAC; Thomason et al., 2018) is used to obtain a typical background aerosol extinction (vertical optical depth of 0.00534 at 675 nm).

As noted in previous polarized RTM intercomparisons (e.g., Emde et al., 2015), the Stokes vectors returned by each RTM are not directly comparable due to differing conventions. A full discussion of the different conventions for reporting the Stokes vector is beyond the scope of this study, and we refer to documentation on each model for specifics on how each individual RTM defines the Stokes vector. For consistency in this study all Stokes parameters are converted to follow the definition of Hovenier et al. (2004), which for the

Table 2. The Rayleigh scattering cross section, ozone absorption cross section, and stratospheric aerosol refractive index used for the test cases.

Wavelength [nm]	Rayleigh cross section [cm^2]	Ozone cross section [cm^2]	Aerosol refractive index
300	5.602831×10^{-26}	3.626519×10^{-19}	$1.452272 - 0i$
315	4.549917×10^{-26}	4.218142×10^{-20}	$1.449746 - 0i$
351	2.878846×10^{-26}	1.225798×10^{-22}	$1.449180 - 1.33565 \times 10^{-05}i$
435	1.177405×10^{-26}	8.362497×10^{-23}	$1.434603 - 4.90115 \times 10^{-05}i$
442	$41.102286 \times 10^{-26}$	1.698570×10^{-22}	$1.433675 - 5.10270 \times 10^{-05}i$
525	5.438003×10^{-27}	2.183215×10^{-21}	$1.429252 - 6.51460 \times 10^{-05}i$
600	3.156146×10^{-27}	5.206045×10^{-21}	$1.429088 - 6.46200 \times 10^{-05}i$
675	1.957387×10^{-27}	1.505802×10^{-21}	$1.428480 - 5.44275 \times 10^{-05}i$
943	5.069933×10^{-28}	0	$1.423274 - 0i$
1020	3.692419×10^{-28}	0	$1.421113 - 0i$
1700	4.611621×10^{-29}	0	$1.396316 - 4.33650 \times 10^{-04}i$

Table 3. Sign that each model's Stokes parameters were multiplied by to follow the definition of Hovenier et al. (2004). A "−" indicates that the component was multiplied by −1, while a "+" indicates the component was unchanged.

Model	Q	U
GSLS	−	+
MYSTIC	+	−
SASKTRAN (MC/HR)	−	+
SCIATRAN	+	+
Siro	−	+
SMART-G	+	−

models included differs only by the sign of Q, U, and/or V. The signs applied to the Stokes parameters from each of the models are shown in Table 3. We define a Cartesian coordinate system z (vertical), x (south), and y (east); the reference frame for the Stokes vector is then the plane spanned by the z and line-of-sight directions. In this frame Q is the "vertical" polarization and U is the "horizontal" polarization.

3.1 A note on atmospheric gridding

The test cases specify the atmospheric state parameters on a 1 km grid from 0 to 100 km but leave the interpolation scheme up to the individual RTM. The two standard choices assume that either the atmospheric state (number densities of various species, temperature, and pressure) varies linearly between grid points or the atmosphere consists of 1 km homogeneous layers where the atmospheric state parameters are constant. How the discretized atmospheric state maps to an effective continuous quantity is of particular importance since any retrieved quantity must be interpreted the same way.

The RTMs GSLS, SASKTRAN (HR and MC), and Siro assume linear interpolation and handle it through analytic methods. All four models calculate optical depth exactly, assuming a linearly varying extinction (see Oikarinen et al., 1999; Loughman et al., 2015, for more details). For SASKTRAN-MC and Siro this is all that is required, and the linear variation in the atmosphere is accounted for without approximation. GSLS and SASKTRAN-HR must make additional approximations in the calculation of the source function, and we refer back to Loughman et al. (2015) and Zawada et al. (2015), respectively, for the exact methods used.

The other RTMs (MYSTIC, SCIATRAN, SMART-G) use homogeneous layers. To better harmonize the treatment of the input data, the RTMs using homogeneous layers have been configured using sub-layers with linear interpolation. Figure 2 shows an example of how using 1000 m or 250 m homogeneous shells varies compared to 100 m shells within MYSTIC. Layering using 1000 m shells introduces errors on the order of 0.5 % at 351 nm in regions where the atmosphere is optically thin, while the error using 250 m shells is 0.1 %. For all future calculations both MYSTIC and SMART-G have been configured to use 250 m shells. SCIATRAN uses a hybrid system where sub-gridding is applied only to the first three layers near the beginning of each integration line and three layers above the tangent point (the exact number of layers is an input parameter).

4 Discussion and results

The main challenge in interpreting and attributing differences between models is that the true answer is not known. All comparisons shown in this section are relative to what we have called the multi-model mean (MMM). The MMM is composed of the set of models that agree with each other to a level that cannot be attributed to a concrete difference in a single model. For the single-scattering test cases the level was determined to be 0.2 %, and 1 % was determined for the multiple-scattering test cases. Any RTM that is found to have

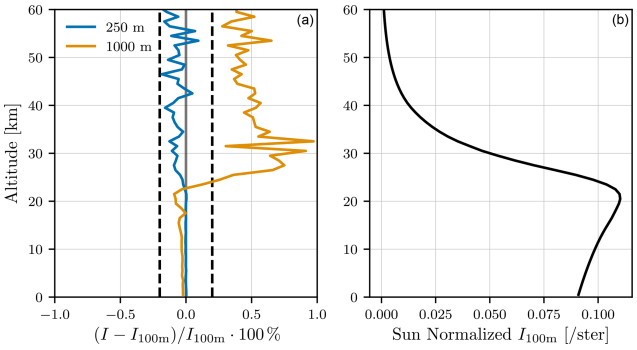

Figure 2. **(a)** Percent difference in single-scattered radiance at 351 nm when MYSTIC is using 1000 m or 250 m homogeneous shells compared to 100 m homogeneous shells. **(b)** The sun-normalized radiance computed using 100 m shells. The atmosphere contains Rayleigh scattering, ozone absorption, and stratospheric aerosol Mie scattering with a SZA of 70°and a SAA of 30°. Refraction is disabled. MYSTIC was configured to use 100 million photons. Dashed vertical lines indicate ±0.2 % levels.

disagreements above these levels is excluded from the MMM for the relevant test case, causing the models composing the MMM to vary between different test cases.

While tests were performed for both vectorial and scalar modes, no significant differences were found in agreement between the models in scalar or vectorial mode. Therefore, for the purpose of brevity, no comparisons of strictly scalar mode are shown. It is understood that the results for the polarized comparisons are equally applicable to scalar calculations.

4.1 Single scatter

Simplifying assumptions made for the single-scatter calculation are minimal, and thus we expect differences to be relatively small. We do not expect zero differences due to the various methods of gridding in the vertical dimension of the atmosphere. As originally done in the limb geometry by Siro (Oikarinen et al., 1999) and discussed extensively in Loughman et al. (2004, 2015), the calculation of optical depth may be performed analytically assuming an extinction that varies linearly in altitude. However, the integration of the source function cannot be performed the same way, and an approximation must be made. For example, SASKTRAN-HR creates a second-order spline of the source function across an integration cell (Zawada et al., 2015), but other models may assume a constant source function or do something more sophisticated. All of this is further complicated by any form of sub-gridding the model may perform in order to obtain a more accurate result.

Differences for the most extreme single-scatter case (Rayleigh + ozone + stratospheric aerosol) are shown in Fig. 3. Differences are presented relative to the mean of the three deterministic models (SASKTRAN-HR, GSLS, and SCIATRAN), which we refer to as the MMM for this case. We chose to use the deterministic models as the reference because statistical errors in the single-scatter case are on the order of the differences observed between the different models. For all conditions, errors between the three deterministic models are less than 0.1 %. The differences between GSLS, SASKTRAN-HR, and SCIATRAN are likely due to the slightly different gridding techniques. For the statistical models MYSTIC, SASKTRAN-MC, SMART-G, and Siro, no errors are detected that are greater than the random noise present ($\sim 0.2\,\%$ in most cases). One thing to note about the SMART-G calculation is that statistical errors are correlated with solar geometry, while for the other MC models the errors are uncorrelated. Errors are correlated because the SMART-G calculation considered multiple solar positions simultaneously in a single simulation, while the other models performed each line of sight and solar position independently.

The excellent agreement in single scatter is expected due to the relative simplicity of the calculation. Fundamentally each RTM solves the single-scatter problem in the same way with minimal assumptions. The primary purpose of this test is to ensure that the inputs to RTM are configured correctly. The agreement of 0.1 %–0.2 % here sets a baseline that differences above this level in more complex test cases cannot be explained by different treatments of input data.

4.2 Multiple scatter

Differences in radiance with multiple scattering enabled are expected to be larger than those seen in single scatter owing to the extra complexity of the radiative transfer problem. The discrete models must deal with discretizations of the multiple-scattering source term and may also make fundamental approximations for the sake of computational speed. Comparatively the statistical models employ a simpler technique.

In Fig. 4 we see that differences between each RTM and the MMM (MYSTIC, SASKTRAN-HR, SASKTRAN-MC, SCIATRAN, and SMART-G) are usually less than 1 % with a few exceptions. Siro shows a low bias on the order of 1 %–4 % at 351 nm, which is most pronounced at low solar zenith angles. The bias is not present when the Lambertian surface albedo is set to 0 instead of 1. This bias was present in Loughman et al. (2004); however it was misattributed to a high bias in the other RTMs as Siro was used as the reference model. Internal testing suggests that the difference may not be directly related to ground scattering and instead is an error that compounds on each successively higher order of scatter. The error is strongest near 351 nm and a surface albedo of 1 because this is the condition where higher orders of scatter have the largest contribution to the observed radiance.

GSLS at 351 nm has a distinct pattern in altitude with variations on the order of 1 % that are relatively consistent across solar geometry. The exact cause of these variations

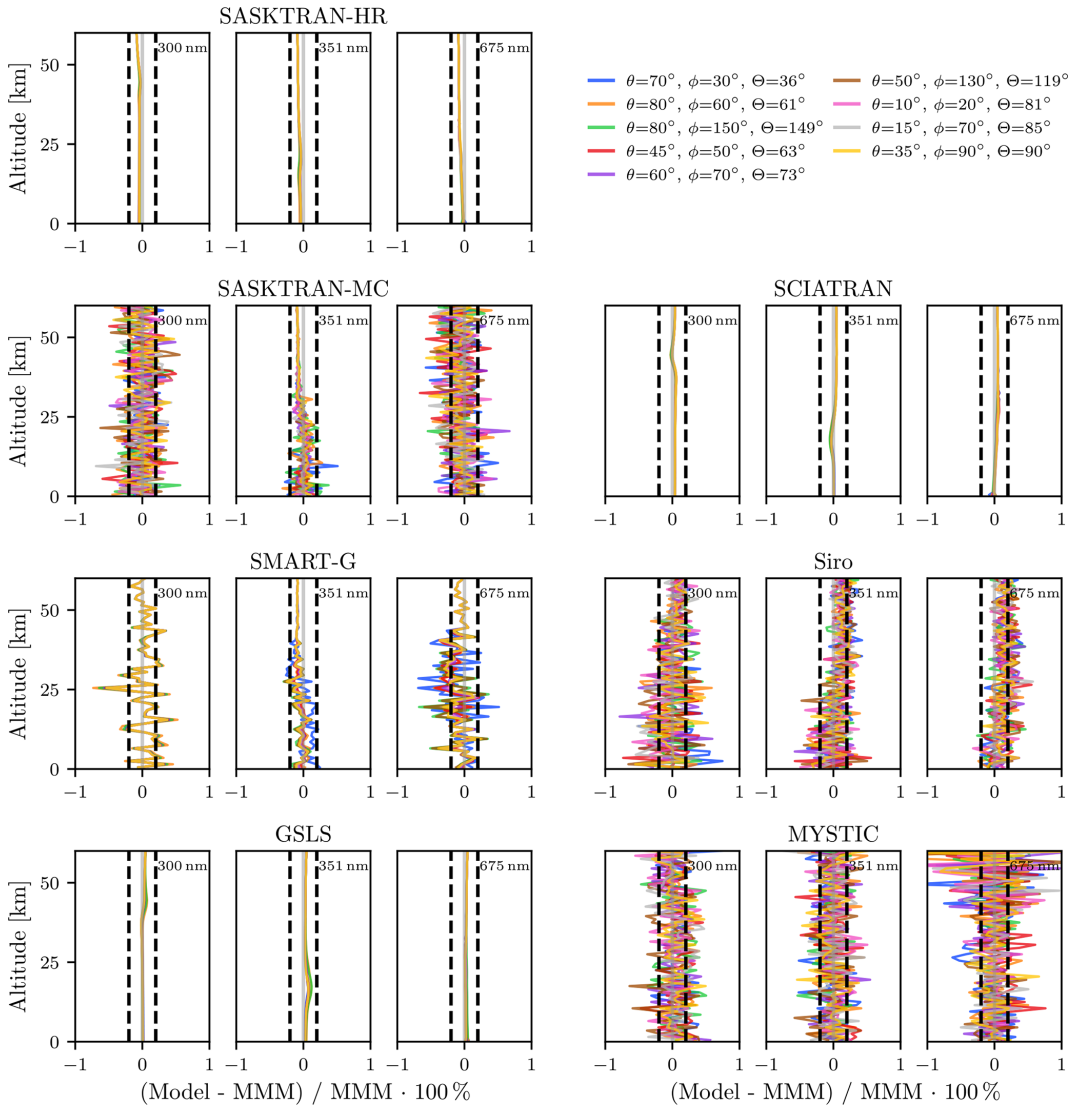

Figure 3. Percent differences in single scatter I relative to the MMM (GSLS, SASKTRAN-HR, and SCIATRAN) for each RTM at a variety of wavelengths and solar conditions. The atmospheric optical properties include Rayleigh scattering, ozone absorption, and stratospheric aerosol Mie scattering. Refraction is disabled. Dashed vertical lines indicate ±0.2 %.

is unknown but is likely caused by discretizations of the multiple-scatter source field calculation; however as stated these variations are fairly small. At 675 nm GSLS shows significant deviations of up to 4 % depending on the solar geometry at altitudes near 25 km. The deviation is only present when the Lambertian surface albedo is 1 and is almost nonexistent with a 0 albedo. Testing has shown that the difference is present for all atmospheric composition scenarios and is thought to be due to approximations made in the ground to line-of-sight multiple-scatter calculation and is currently under investigation.

SASKTRAN (HR and MC), SCIATRAN, SMART-G, and MYSTIC all agree for all conditions to better than 1 %. As stated, differences less than 1 % are difficult to attribute to any particular RTM due to both not having a precise reference model and the inherent statistical noise. However, we do note that SASKTRAN-HR and SCIATRAN both have altitude variation patterns on the order of 0.5 % that are constant across solar geometry but differ in wavelength. MYSTIC, SASKTRAN-MC, and SMART-G are indistinguishable at the level of statistical noise. We have found no differences that are indicative of differences in stratospheric aerosol scattering. Differences at longer wavelengths (not shown) are comparable to those at 675 nm, where aerosol scattering can make up ∼ 75 % of the observed signal in the forward scatter high-albedo case. The general agreement between the models is better than has been observed before in comparisons of RTMs in limb scatter geometry even for scalar cases.

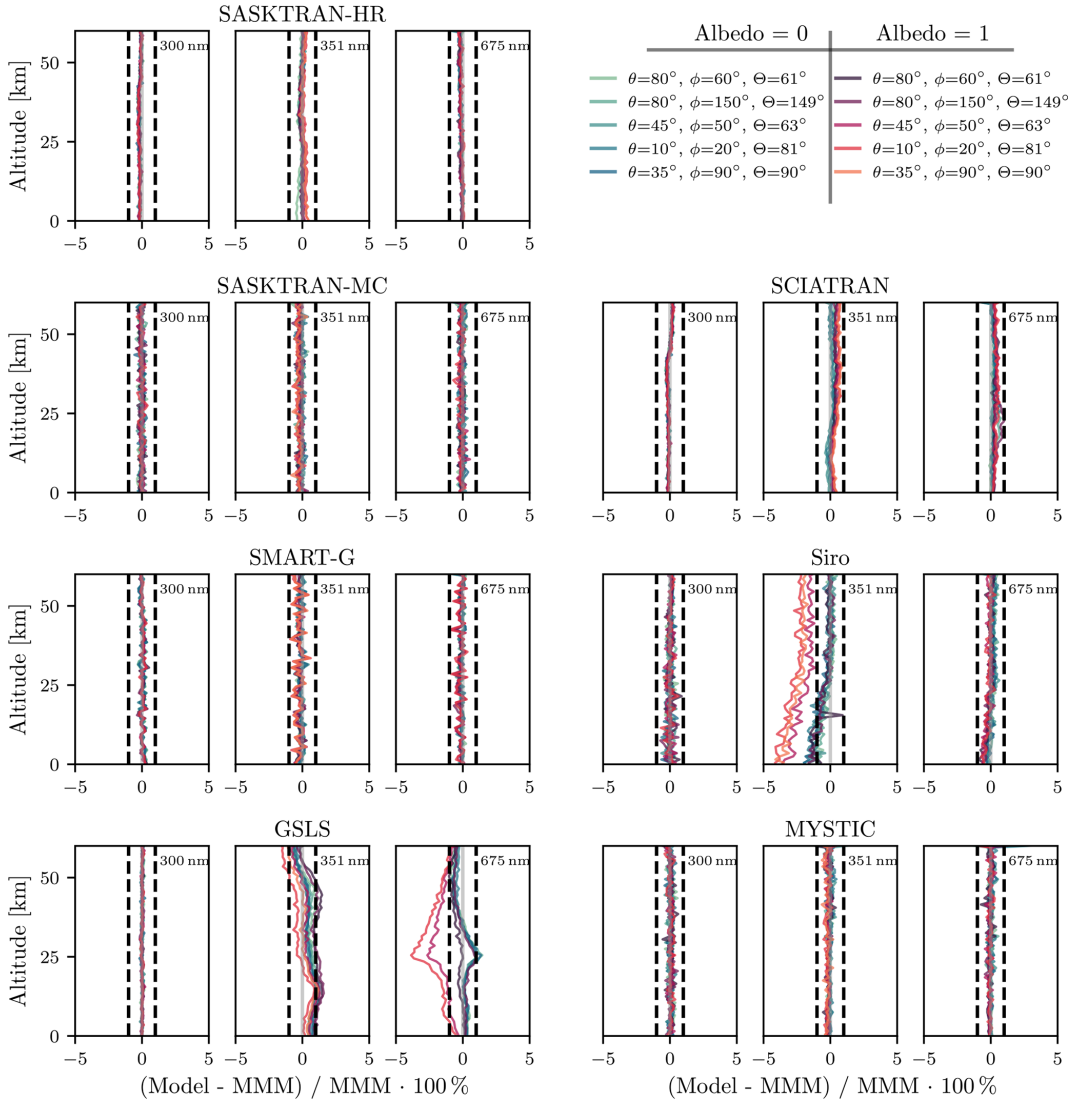

Figure 4. Percent differences in I, with multiple scattering enabled, relative to the MMM (MYSTIC, SASKTRAN-HR, SASKTRAN-MC, SCIATRAN, and SMART-G) for each RTM at a variety of wavelengths and solar conditions. The atmospheric optical properties include Rayleigh scattering, ozone absorption, and stratospheric aerosol Mie scattering. Refraction is disabled. Dashed vertical lines indicate ±1 % levels.

4.3 Stokes parameters

While all comparisons so far have involved vector radiative transfer calculations, only differences in the I component of the Stokes vector have been analyzed. Agreement in I is indicative that the polarization implementation in each model is sensible; however polarization can be investigated more rigorously by analyzing the individual Stokes parameters. Figure 5 shows the individual Stokes components and their differences to the MMM (MYSTIC, SMART-G, and SASKTRAN-MC) for one scenario with large polarization (scattering angle near 90°, albedo 0) and one scenario with low polarization (scattering angle away from 90°, albedo 1).

Generally agreement between Q, U, and the linear polarization, $\sqrt{Q^2+U^2}$, is worse than the agreement with I. MYSTIC, SASKTRAN-MC, and SMART-G agree for all components at the level of statistical noise (∼ 0.2 %–1 %), while Siro shows deviations at altitudes below 30 km that can approach 5 % depending on the condition. SASKTRAN-HR and SCIATRAN are usually within 1 % for the cases shown; however in some situations this can exceed 1 %. In cases where the polarization is small, GSLS can show deviations of 2 %–4 %, but these disappear in the cases with high linear polarization. The differences observed in linear polarization sometimes mirror differences observed in I and are sometimes independent.

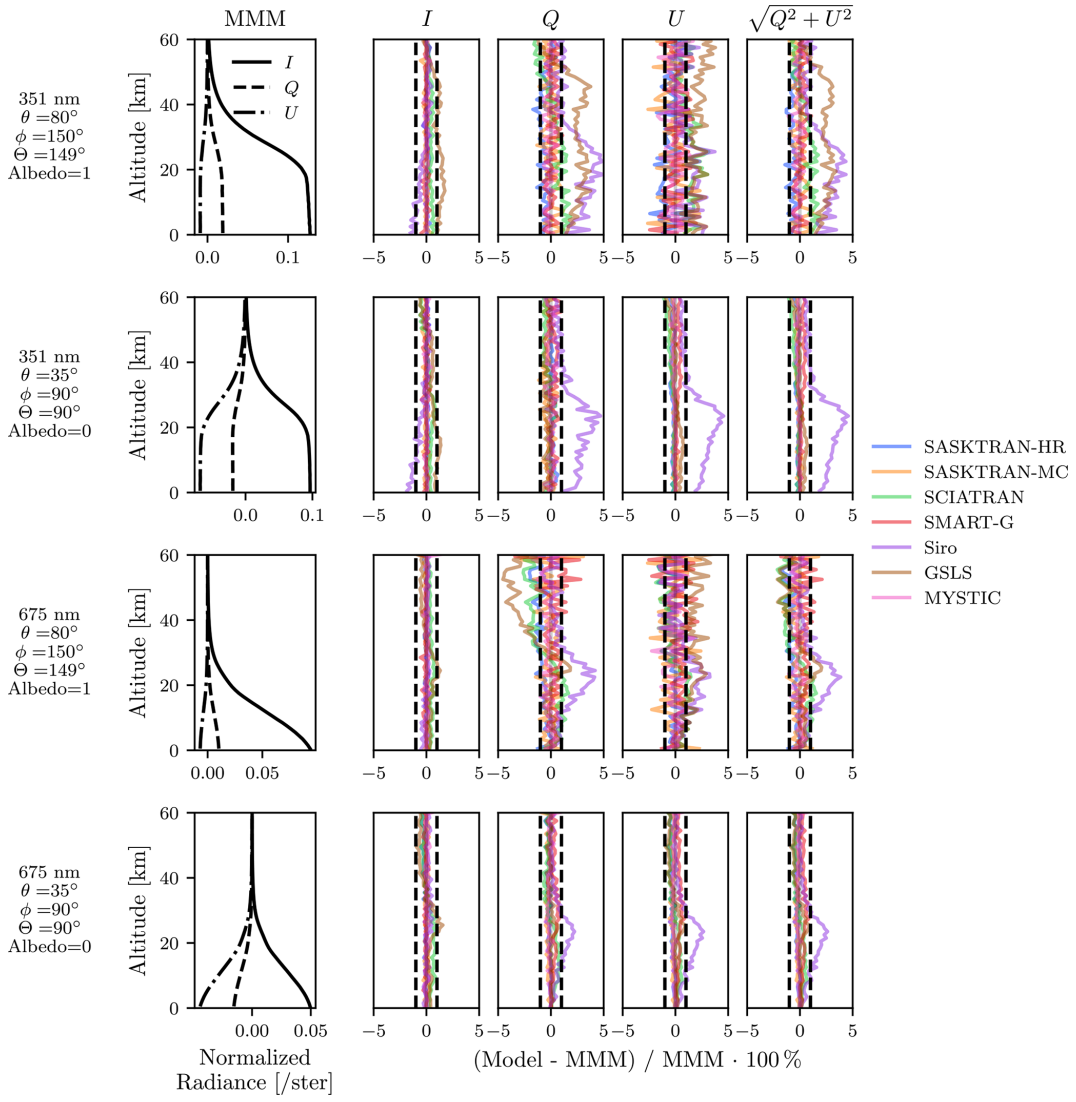

Figure 5. Leftmost column: the MMM calculation of I, Q, and U for four different scenarios consisting of MYSTIC, SASKTRAN-MC, and SMART-G. Other columns: percent difference in I, Q, U, and $\sqrt{Q^2+U^2}$ for each model relative to the MMM. The atmospheric optical properties include Rayleigh scattering, ozone absorption, and aerosol scattering. Dashed vertical lines indicate ±1 % levels.

In order to isolate the polarization effects, we consider two quantities: the degree of linear polarization (DOLP) and the linear polarization orientation (LPO). DOLP is defined as

$$\mathrm{DOLP} = \frac{\sqrt{Q^2+U^2}}{I}, \tag{1}$$

which is the fraction of radiation that is linearly polarized, and LPO is defined as

$$\mathrm{LPO} = \frac{1}{2}\arctan\frac{U}{Q}, \tag{2}$$

which indicates the direction of linear polarization. The absolute differences in DOLP and LPO for the Rayleigh scattering, ozone absorption, and stratospheric aerosol scattering case are shown in Figs. 6 and 7, respectively.

Differences in the DOLP and LPO are overall small, with a few exceptions. Once again, the MC models MYSTIC, SASKTRAN-MC, and SMART-G agree in all cases to the level of statistical noise in the computation. At 300 nm no differences are observed between the models as the majority of the signal is single scatter. GSLS, SASKTRAN-HR, and SCIATRAN all have minor spreads in DOLP at 351 nm depending on solar angle and albedo on the order of 0.002. SCIATRAN shows differences in LPO at 351 nm of 0.2° for some conditions; however these are conditions where the overall polarization signal is small. At 675 nm GSLS has differences in DOLP of up to 0.02 when the surface albedo is 1, which are likely related to the differences in I observed previously. For the same wavelength the LPO shows deviations on the order of 0.5° for the high-surface-albedo case.

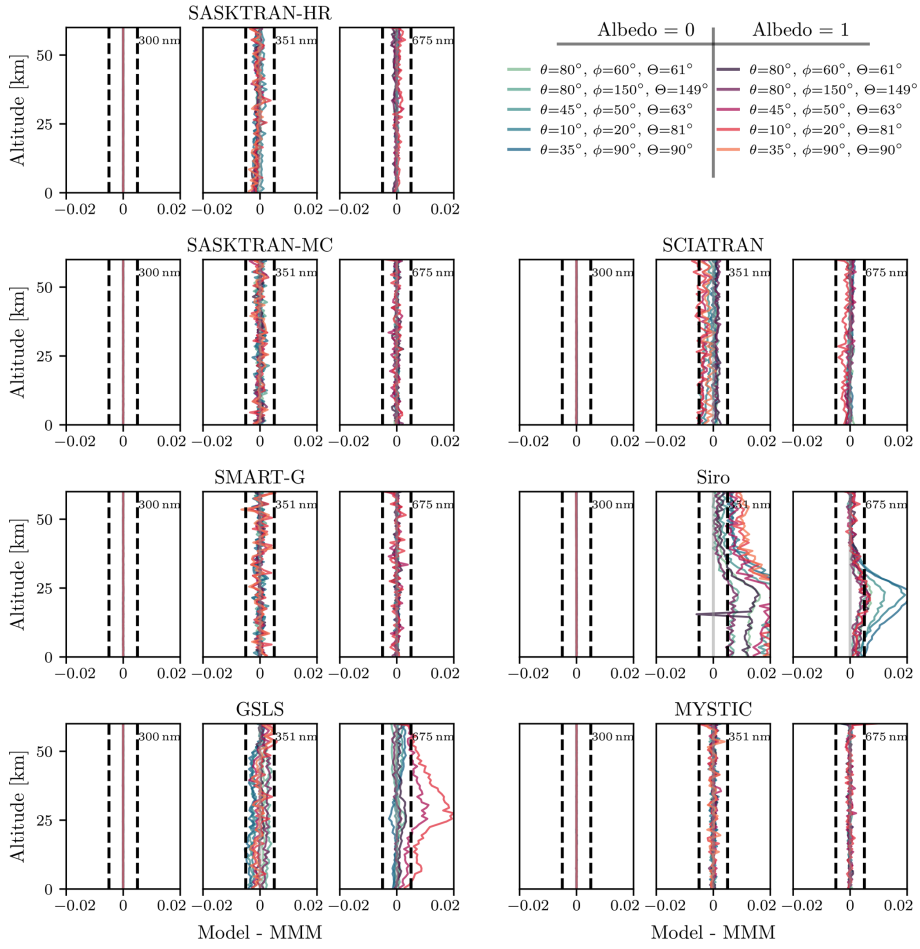

Figure 6. Absolute differences in DOLP relative to the MMM (MYSTIC, SASKTRAN-MC, and SMART-G) for each RTM at a variety of wavelengths and solar conditions. The atmospheric optical properties include Rayleigh scattering, ozone absorption, and stratospheric aerosol Mie scattering. Refraction is disabled. Dashed vertical lines indicate ±0.005 levels.

Siro has differences in DOLP but curiously does not have any significant differences in LPO. At 351 nm, deviations in DOLP are up to 0.03 and are present at all albedos and solar conditions but are larger at high albedo and low solar zenith angle. The deviations are largest at conditions where there were significant differences in I but do not share the same shape. There are differences of up to 0.02 at 675 nm in DOLP between Siro and the MMM; however the differences are only present at low albedos. The differences are largely eliminated when aerosol is removed from the atmosphere (not shown), suggesting that it could be due to aerosol multiple scattering.

Both SASKTRAN (HR and MC) and GSLS make the assumption that V is exactly 0, which reduces the size of the phase matrix to speed up the computation, and it does not appear that this approximation affects the results in a noticeable way. The approximation is not fundamental to the method of solution used by SASKTRAN (HR and MC) and GSLS, but currently the models do not have an option to remove it. The comparison atmospheres only include smaller spherical scatterers (Mie and Rayleigh scattering) and do not include larger particles as would be seen in ice clouds for example. It is possible that the approximation of neglecting V would break down under conditions containing larger particles, droplets, or crystals where there is greater coupling between linear and circular polarization. These cases are a subject of potential future study.

4.4 Refraction

All of the models considered thus far with the exceptions of SASKTRAN-MC and MYSTIC support atmospheric refraction to some level. While Siro has support for refraction, it was not tested as part of this study. GSLS and SASKTRAN-HR neglect refraction of the incoming solar rays. Furthermore GSLS and SASKTRAN-HR neglect refraction for multiple-scattering effects, only implementing refraction for the line-of-sight ray. SCIATRAN and SMART-G implement refraction in a generic way accounting for all solar and multiple-scattering effects. SASKTRAN-HR has

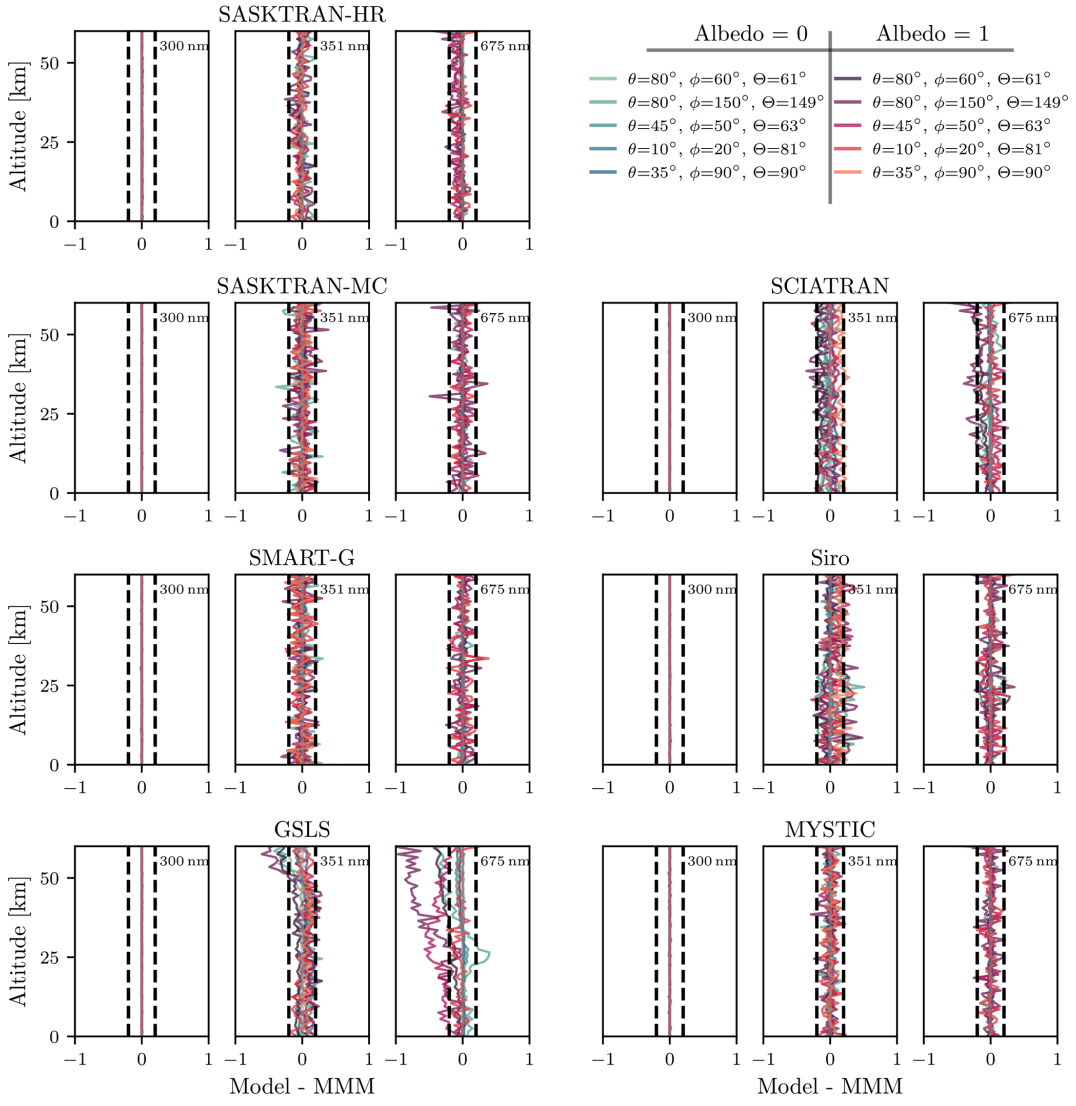

Figure 7. Absolute differences in LPO [°] relative to the MMM (MYSTIC, SASKTRAN-MC, and SMART-G) for each RTM at a variety of wavelengths and solar conditions. The atmospheric optical properties include Rayleigh scattering, ozone absorption, and stratospheric aerosol Mie scattering. Refraction is disabled. Dashed vertical lines indicate ±0.2° levels.

since been updated to include refractive effects for incoming solar rays and multiple-scatter effects, but the calculations here use only line-of-sight refraction.

Differences in radiance when refraction is enabled for the stratospheric aerosol scattering case are shown in Fig. 8. At 351 nm the effect of refraction is minimal, and agreement is identical to the cases without refraction; however, at longer wavelengths several differences are observed between the RTMs. SMART-G has a discontinuity in the signal at 11.5 km, causing differences on the order of 1 % relative to SASKTRAN-HR and SCIATRAN. The agreement of GSLS relative to the other models is almost identical in the refracted and unrefracted cases, indicating that the refractive effect is similar to that of SASKTRAN-HR and SCIATRAN.

To further investigate these differences, the ratio of refracted to unrefracted I for a single condition for each model is shown in Fig. 9. This refraction ratio was found to be insensitive to the solar geometry, albedo, and atmospheric composition. At short wavelengths and low tangent altitudes, the increased extinction causes the atmosphere to be optically thick, reducing the contribution from the lower atmospheric layers where the refractive effects are significant. Therefore the refraction ratio is shown at 1020 nm, which is representative of the differences observed between the models at all wavelengths where the atmosphere is optically thin. GSLS, SASKTRAN-HR, and SCIATRAN show excellent agreement in the refraction ratio, with differences being insignificant next to the already observed differences between the models. The refractive enhancement in SMART-G is 1–

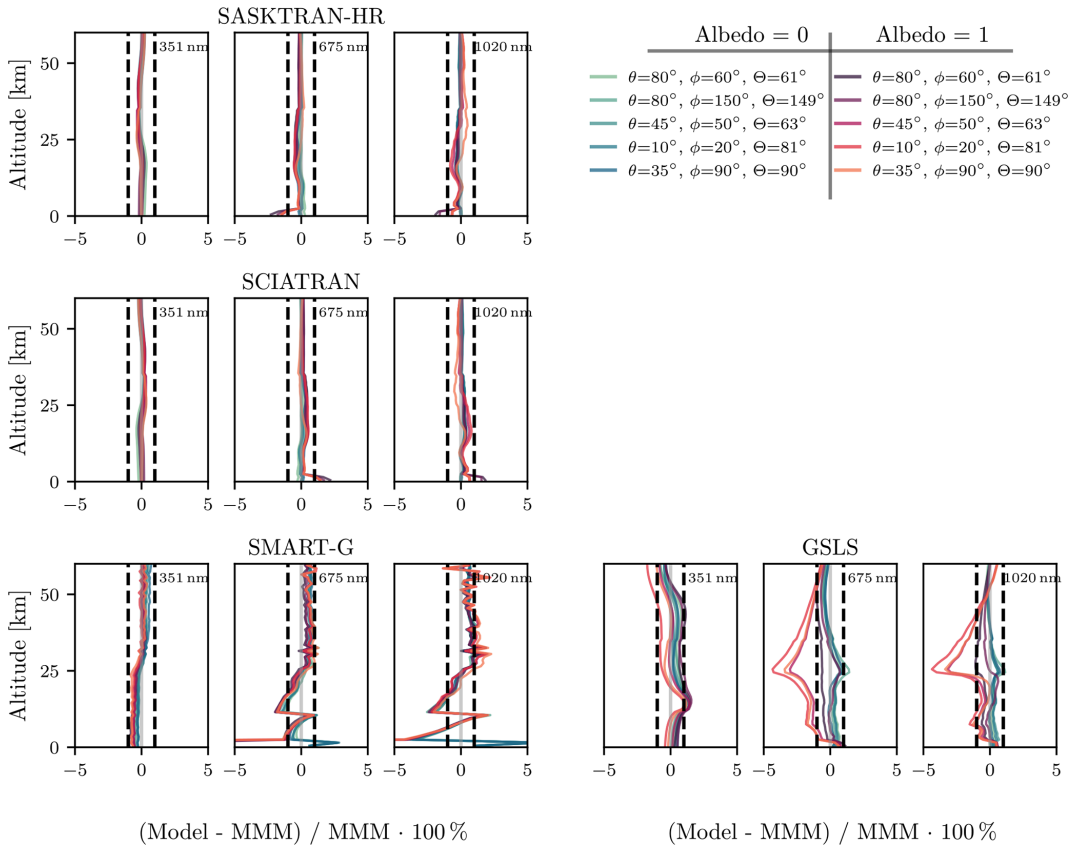

Figure 8. Same as Fig. 4 but with refraction enabled. The MMM is composed of SASKTRAN and SCIATRAN. Dashed vertical lines indicate ±1 % levels.

2 % less than GSLS, SASKTRAN-HR, and SCIATRAN with the exception of a discontinuity near 11.5 km that greatly enhances the refractive enhancement for a few kilometers below. Possible reasons for the differences of SMART-G compared to GSLS, SASKTRAN-HR, and SCIATRAN are still under investigation.

There are several possible reasons for the small observed differences between GSLS, SASKTRAN-HR, and SCIATRAN. The index of refraction of the atmosphere was not harmonized between the models; instead each model performed internal calculations using the provided atmospheric temperature and pressure. Various methods exist to do this calculation, and they may not be the same between each RTM. Differing methods of ray tracing and integration can also lead to small differences. Since SCIATRAN (and SMART-G) included refractive effects for the incoming solar ray and multiple-scatter terms, it is possible that solar refraction could be the source of some minor differences. The solar geometries tested here have been limited to SZA $\leq 80°$, where refraction of the incoming solar ray is expected to be minimal. Further study could examine the effect of refraction at larger solar zenith angles.

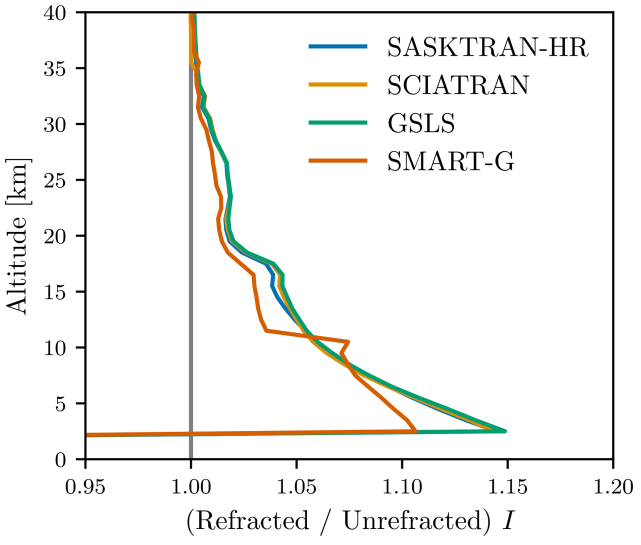

Figure 9. Ratio of refracted to unrefracted I with multiple scattering enabled, Rayleigh scattering + ozone absorption + stratospheric aerosol scattering, SZA = 70°, SAA = 30°, and a Lambertian surface reflectance of 0 at 1020 nm for every model that supports refraction.

4.5 Timing

We have considered a basic run time comparison between the models in the study. While a useful exercise, there are technical challenges in standardizing the hardware used to execute the models, and in the case of SMART-G, which uses a GPU, the standardization is not possible. More importantly every model has settings that involve an accuracy–speed trade-off. For example, with the deterministic models, there are various discretization settings that can dramatically affect the speed of the calculations.

Harmonizing the balance between accuracy and speed between all of the RTMs is impractical; instead we opt for a simple order of magnitude timing estimate. The time taken to execute all of the multiple-scatter-enabled, polarized tests for each model without refraction is shown in Table 4. These timing numbers should be interpreted as the time required to execute a wide variety of test cases, and individual RTMs may be significantly more or less efficient in specific cases. However analyzing these differences is beyond the scope of this study. For the CPU-based models a scaled run time value is also supplied where the run time on equivalent hardware has been approximated using the relative multithreaded CPU benchmark values from https://www.passmark.com/ (last access: 6 November 2020). The deterministic models, GSLS, SCIATRAN, and SASKTRAN-HR, all have run times of a similar order of magnitude taking anywhere from 0.3 to 1 s to execute a single wavelength, solar geometry, and atmospheric composition on average.

Analyzing the timing of the Monte Carlo models is inherently more challenging as the calculations also contain statistical noise. It is common to benchmark models for a set number of photons; however the number of photons used is not comparable between Siro/SASKTRAN-MC and MYSTIC/SMART-G since the MC technique is not the same. Instead, the precision of the calculation must be directly compared, which is shown for a typical condition in Fig. 10. For the precision estimation and timing, MYSTIC was configured to use a constant 1E6 photons. The other models (SASKTRAN-MC, Siro, and SMART-G) were configured identically to the previous radiance comparisons. Siro used a constant 1E6 photons, while SASKTRAN-MC and SMART-G used a variable number of photons targeting 0.2 %–0.3 % precision.

For the given precisions, the CPU-based statistical models, MYSTIC, SASKTRAN-MC, and Siro, have run times within an order of magnitude. The run time of Siro appears large; however the precision is generally better. Approximately scaling the Siro calculation to 0.2 % precision would result in a speed increase of a factor of ~ 4. Because of the differences in precision between the different calculations, we won't attempt to quantify small differences between the MC models. One thing of particular interest is the general efficiency between the technique used by Siro–SASKTRAN-MC and MYSTIC–SMART-G. Both Siro and MYSTIC used a constant 1E6 photons for all conditions; however the precision of Siro is relatively constant in altitude and wavelength hovering around 0.1 %, while the precision of MYSTIC varies significantly. MYSTIC achieved better than 0.1 % precision in cases where the atmosphere heavily scatters (low altitudes, shorter wavelengths) and worse precision at higher altitudes and longer wavelengths where the atmosphere is optically thin. As mentioned earlier, this is since photons in Siro are forced to scatter, while photons in MYSTIC may pass through the atmosphere without interaction.

The run time for the GPU-based MC model, SMART-G, is $\sim$ 1–2 orders of magnitude less than the other MC models. The most natural comparison is between SMART-G and SASKTRAN-MC since they have similar precision for this case. Here, SMART-G achieves a speedup of $\sim 30\times$ relative to SASKTRAN-MC on the hardware used. SMART-G improves the relative precision of the calculation by forcing scatter events to happen on the first order of scatter (similar to SASKTRAN-MC and Siro, which force scatters on all orders), and it appears that this is sufficient to obtain reasonable precision in all scenarios.

5 Conclusions

A systematic comparison has been performed between seven radiative transfer models operating in the limb scatter geometry. The seven models are capable of handling the sphericity of the atmosphere and compute the Stokes vector accounting for polarization. The test cases cover a wide variety of solar angles, Rayleigh scattering, ozone absorption, Mie scattering, and surface reflectances.

In single scatter, the deterministic models GSLS, SASKTRAN-HR, and SCIATRAN agree within 0.1 % for all observed conditions. The statistical models MYSTIC, SASKTRAN-MC, Siro, and SMART-G all agree at the level of precision of the calculation, which is approximately ~ 0.2 %.

For almost all conditions with multiple scattering enabled, the agreement between the fully spherical models is within 1 % when refraction is disabled for I with a few exceptions.

- Siro can have disagreement of up to 3 % at shorter wavelengths, particularly when the solar zenith angle is small and the surface reflectance is high. The difference manifests as a low bias in the radiance and a high bias in the degree of linear polarization. The cause of this bias is currently unknown.

- At longer wavelengths in all atmospheric conditions and when the Lambertian surface reflectance is high, GSLS shows biases of up to 3 % that are dependent on solar geometry. The bias is thought to be caused by approximations made in the ground to line-of-sight multiple-scattering calculation but is still under investigation.

Table 4. Estimated time to execute all multiple-scattering-enabled, no-refraction tests. This includes 3 effective surface albedos, 3 different atmospheric compositions, 11 wavelengths, 9 solar geometries, and 80 lines of sight. The MC models were executed to the precision shown in Fig. 10 (see text for more detail).

Model	Hardware description	Time [minutes]	Scaled run time* [minutes]
GSLS	Two Intel Xeon E5-2630 (6 physical cores at 2.3 GHz each)	35	13.0
SASKTRAN-HR	AMD 3900x (12 physical cores at 3.8 GHz)	7.4	7.4
SCIATRAN	Intel i7-6850 (6 physical cores at 3.6 GHz)	13.5	4.6
SASKTRAN-MC	AMD 3900x (12 physical cores at 3.8 GHz)	1909	1909
Siro	Four Intel Xeon E5-2630 (8 physical cores at 2.4 GHz each)	16 560	20 078
MYSTIC	AMD 3900x (12 physical cores at 3.8 GHz)	1906	1906
SMART-G	NVIDIA Titan V	59.2	Not applicable

* The scaled run time is calculated by scaling every CPU to the computational power of the AMD 3900x using the relative benchmark values from https://www.passmark.com/ (last access: 6 November 2020) as of 6 November 2020.

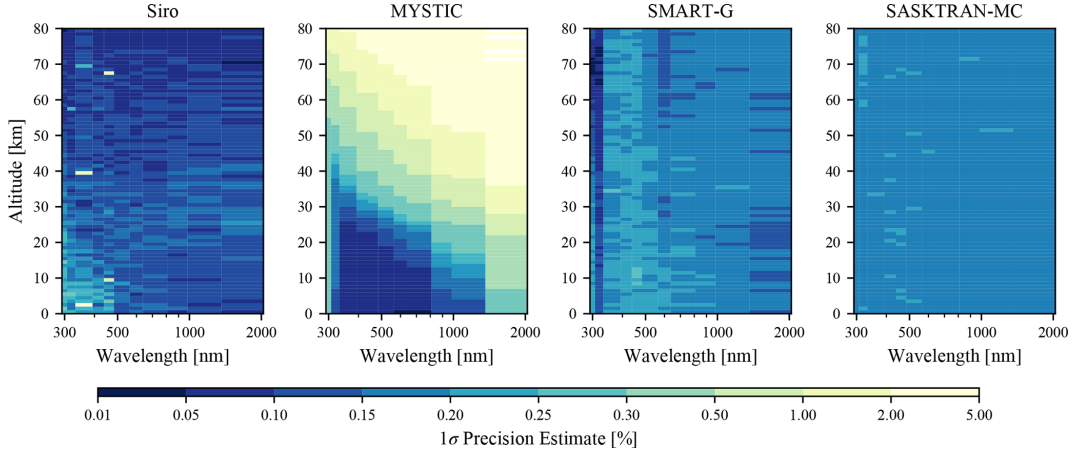

Figure 10. Precision estimates for the MC models with multiple scattering, Rayleigh scattering + ozone absorption + stratospheric aerosol scattering, SZA = 70°, SAA = 30°, and a Lambertian surface reflectance of 1. Precision estimates for MYSTIC, SASKTRAN-MC, and SMART-G were taken from the model output. Siro precision was estimated by running the above scenario 20 times and taking the standard deviation.

Refraction has been tested for GSLS, SASKTRAN-HR, SMART-G, and SCIATRAN. The refractive effect among all models is almost indistinguishable, with the exception of a ~ 1 % jump in radiance in the SMART-G calculation at 11.5 km when refraction is enabled. The cause of the jump is currently unknown.

Differences in quantities representing linear polarization, the DOLP and LPO, have also been assessed; however the results are more difficult to interpret. The MC models MYSTIC, SASKTRAN-MC, and SMART-G agree within statistical noise for all considered conditions and serve as a combined reference. SASKTRAN-HR and SCIATRAN generally agree with the reference at a level of 0.002 in DOLP and 0.2° in LPO, with the largest deviations in LPO being in conditions where the linearly polarized signal is small. For most conditions, GSLS agrees at a similar level, with the exception of high Lambertian surface albedos at longer wavelengths where DOLP can vary up to 0.02 and LPO by 0.5°. Siro shows deviations in DOLP at both 351 and 675 nm that approach 0.03 but has no distinguishable difference from the reference in LPO.

Overall the agreement between the models is excellent and is better than has been reported for scalar comparisons in the past. The agreement provides additional confidence in the retrievals from limb scatter instruments such as OMPS-LP, OSIRIS, and SCIAMACHY. In particular, confidence in modeling the polarized signal is important for the upcoming ALTIUS mission.

There are several areas where future studies comparing RTMs in the limb-viewing geometry could expand upon. Scattering from larger, non-spherical, particles, droplets, or crystals such as those contained in clouds should be assessed, which may result in larger differences in particular for circular polarization. More extreme cases with higher solar zenith angles may be checked to further push the models, which could also be used to determine the effect of refraction at

higher solar zenith angles. Non-Lambertian reflecting surfaces as well as a larger variety of stratospheric aerosol conditions would be another interesting area of study. Finally, the impact of the observed differences between the models could be studied in the context of standard applications such as limb scatter species retrievals.

Data availability. The input atmospheric data, test cases, and the results for each model are made publicly available as https://doi.org/10.5281/zenodo.4292303 (Zawada et al., 2020).

Author contributions. DZ wrote the initial draft of the manuscript. Model runs were performed by DZ, GF, RL, AM, and AR. All authors contributed in designing the study, interpreting the results, and revising the manuscript.

Competing interests. The authors declare that they have no conflict of interest.

Special issue statement. This article is part of the special issue "New developments in atmospheric limb measurements: instruments, methods, and science applications (AMT/ACP inter-journal SI)". It is a result of the 10th international limb workshop, Greifswald, Germany, 4–7 June 2019.

Acknowledgements. Robert Loughman appreciates the support of Ghassan Taha and Tong Zhu for the code testing work done for this project. Dan Kahn, Jason Li, Mike Linda, and Colin Seftor also provided valuable assistance with NASA computer access, code setup, and timing assessments, while Surendra Bhatta contributed Python programming assistance. The manuscript was greatly improved by the helpful suggestions of the two reviewers (Christopher Sioris and Chris McLinden) as well as those from Sergey Korkin.

Financial support. The work has been partially supported by the Canadian Space Agency, the European Space Agency, the state of Bremen and the University of Bremen. Advancements of the radiative transfer model SCIATRAN made are a contribution to the project VolARC funded by the German Research Foundation (DFG) through the research unit VolImpact (grant no. FOR2820). The work by Antti Mikkonen was supported by the Academy of Finland Centre of Excellence in Inverse Modelling and Imaging (project number 312125). The work of Robert Loughman was funded by NASA contract (grant no. 80NSSC18K0847; led by Ghassan Taha).

Review statement. This paper was edited by Chris McLinden and reviewed by Chris Sioris and Chris McLinden.

References

Arosio, C., Rozanov, A., Malinina, E., Eichmann, K.-U., von Clarmann, T., and Burrows, J. P.: Retrieval of ozone profiles from OMPS limb scattering observations, Atmos. Meas. Tech., 11, 2135–2149, https://doi.org/10.5194/amt-11-2135-2018, 2018.

Bernath, P. F., McElroy, C. T., Abrams, M. C., Boone, C. D., Butler, M., Camy-Peyret, C., Carleer, M., Clerbaux, C., Coheur, P. F., Colin, R., DeCola, P., DeMazière, M., Drummond, J. R., Dufour, D., Evans, W. F., Fast, H., Fussen, D., Gilbert, K., Jennings, D. E., Llewellyn, E. J., Lowe, R. P., Mahieu, E., McConnell, J. C., McHugh, M., McLeod, S. D., Michaud, R., Midwinter, C., Nassar, R., Nichitiu, F., Nowlan, C., Rinsland, C. P., Rochon, Y. J., Rowlands, N., Semeniuk, K., Simon, P., Skelton, R., Sloan, J. J., Soucy, M. A., Strong, K., Tremblay, P., Turnbull, D., Walker, K. A., Walkty, I., Wardle, D. A., Wehrle, V., Zander, R., and Zou, J.: Atmospheric chemistry experiment (ACE): Mission overview, Geophys. Res. Lett., 32, L15S01, https://doi.org/10.1029/2005GL022386, 2005.

Bourassa, A. E., Degenstein, D. A., Gattinger, R. L., and Llewellyn, E. J.: Stratospheric aerosol retrieval with optical spectrograph and infrared imaging system limb scatter measurements, J. Geophys. Res., 112, D10217, https://doi.org/10.1029/2006JD008079, 2007.

Bourassa, A. E., Degenstein, D. A., and Llewellyn, E. J.: SASKTRAN: A spherical geometry radiative transfer code for efficient estimation of limb scattered sunlight, J. Quant. Spectrosc. Ra., 109, 52–73, https://doi.org/10.1016/j.jqsrt.2007.07.007, 2008.

Bovensmann, H.: SCIAMACHY: Mission objectives and measurement modes, J. Atmos. Sci., 56, 127–150, 1999.

Brion, J., Chakir, A., Daumont, D., Malicet, J., and Parisse, C.: High-resolution laboratory absorption cross section of O_3. Temperature effect, Chem. Phys. Lett., 213, 610–612, 1993.

Buras, R. and Mayer, B.: Efficient unbiased variance reduction techniques for Monte Carlo simulations of radiative transfer in cloudy atmospheres: The solution, J. Quant. Spectrosc. Ra., 112, 434–447, https://doi.org/10.1016/j.jqsrt.2010.10.005, 2011.

Butz, A., Bösch, H., Camy-Peyret, C., Chipperfield, M., Dorf, M., Dufour, G., Grunow, K., Jeseck, P., Kühl, S., Payan, S., Pepin, I., Pukite, J., Rozanov, A., von Savigny, C., Sioris, C., Wagner, T., Weidner, F., and Pfeilsticker, K.: Inter-comparison of stratospheric O_3 and NO_2 abundances retrieved from balloon borne direct sun observations and Envisat/SCIAMACHY limb measurements, Atmos. Chem. Phys., 6, 1293–1314, https://doi.org/10.5194/acp-6-1293-2006, 2006.

Chowdhary, J., Zhai, P.-W., Boss, E., Dierssen, H., Frouin, R., Ibrahim, A., Lee, Z., Remer, L. A., Twardowski, M., Xu, F., Zhang, X., Ottaviani, M., Espinosa, W. R., and Ramon, D.: Modeling Atmosphere-Ocean Radiative Transfer: A PACE Mission Perspective, Front. Earth Sci., 7, https://doi.org/10.3389/feart.2019.00100, 2019.

Chowdhary, J., Zhai, P.-W., Xu, F., Frouin, R., and Ramon, D.: Testbed results for scalar and vector radiative transfer computations of light in atmosphere-ocean systems, J. Quant. Spectrosc. Ra., 242, 106717, https://doi.org/10.1016/j.jqsrt.2019.106717, 2020.

Cisewski, M., Zawodny, J., Gasbarre, J., Eckman, R., Topiwala, N., Rodriguez-Alvarez, O., Cheek, D., and Hall, S.: The Stratospheric Aerosol and Gas Experiment (SAGE III) on the International Space Station (ISS) Mission, in: Sensors, Systems, and

Next-Generation Satellites XVIII, SPIE Remote Sensing, Proc. SPIE 9241, 924107, https://doi.org/10.1117/12.2073131, 2014.

Daumont, D., Brion, J., Charbonnier, J., and Malicet, J.: Ozone UV spectroscopy I: Absorption cross-sections at room temperature, J. Atmos. Chem., 15, 145–155, 1992.

Degenstein, D. A., Bourassa, A. E., Roth, C. Z., and Llewellyn, E. J.: Limb scatter ozone retrieval from 10 to 60 km using a multiplicative algebraic reconstruction technique, Atmos. Chem. Phys., 9, 6521–6529, https://doi.org/10.5194/acp-9-6521-2009, 2009.

Dueck, S. R., Bourassa, A. E., and Degenstein, D. A.: An efficient algorithm for polarization in the SASKTRAN radiative transfer framework, J. Quant. Spectrosc. Ra., 199, 1–11, https://doi.org/10.1016/j.jqsrt.2017.05.016, 2017.

Elash, B., Bourassa, A., Rieger, L., Dueck, S., Zawada, D., and Degenstein, D.: The sensitivity to polarization in stratospheric aerosol retrievals from limb scattered sunlight measurements, J. Quant. Spectrosc. Ra., 189, 75–85, https://doi.org/10.1016/j.jqsrt.2016.11.014, 2017.

Elash, B. J., Bourassa, A. E., Loewen, P. R., Lloyd, N. D., and Degenstein, D. A.: The Aerosol Limb Imager: acousto-optic imaging of limb-scattered sunlight for stratospheric aerosol profiling, Atmos. Meas. Tech., 9, 1261–1277, https://doi.org/10.5194/amt-9-1261-2016, 2016.

Emde, C. and Mayer, B.: Simulation of solar radiation during a total eclipse: a challenge for radiative transfer, Atmos. Chem. Phys., 7, 2259–2270, https://doi.org/10.5194/acp-7-2259-2007, 2007.

Emde, C., Buras, R., Mayer, B., and Blumthaler, M.: The impact of aerosols on polarized sky radiance: model development, validation, and applications, Atmos. Chem. Phys., 10, 383–396, https://doi.org/10.5194/acp-10-383-2010, 2010.

Emde, C., Buras, R., and Mayer, B.: ALIS: An efficient method to compute high spectral resolution polarized solar radiances using the Monte Carlo approach, J. Quant. Spectrosc. Ra., 112, 1622–1631, https://doi.org/10.1016/j.jqsrt.2011.03.018, 2011.

Emde, C., Barlakas, V., Cornet, C., Evans, F., Korkin, S., Ota, Y., Labonnote, L. C., Lyapustin, A., Macke, A., Mayer, B., and Wendisch, M.: IPRT polarized radiative transfer model intercomparison project – Phase A, J. Quant. Spectrosc. Ra., 164, 8–36, https://doi.org/10.1016/j.jqsrt.2015.05.007, 2015.

Emde, C., Buras-Schnell, R., Kylling, A., Mayer, B., Gasteiger, J., Hamann, U., Kylling, J., Richter, B., Pause, C., Dowling, T., and Bugliaro, L.: The libRadtran software package for radiative transfer calculations (version 2.0.1), Geosci. Model Dev., 9, 1647–1672, https://doi.org/10.5194/gmd-9-1647-2016, 2016.

Emde, C., Buras-Schnell, R., Sterzik, M., and Bagnulo, S.: Influence of aerosols, clouds, and sunglint on polarization spectra of Earthshine, Astron. Astrophys., 605, A2, https://doi.org/10.1051/0004-6361/201629948, 2017.

Emde, C., Barlakas, V., Cornet, C., Evans, F., Wang, Z., Labonotte, L. C., Macke, A., Mayer, B., and Wendisch, M.: IPRT polarized radiative transfer model intercomparison project – Three-dimensional test cases (phase B), J. Quant. Spectrosc. Ra., 209, 19–44, https://doi.org/10.1016/J.JQSRT.2018.01.024, 2018.

Flynn, L. E., Seftor, C. J., Larsen, J. C., and Xu, P.: The ozone mapping and profiler suite, in: Earth science satellite remote sensing, Springer, Berlin, Heidelberg, 279–296, 2006.

Fussen, D., Baker, N., Debosscher, J., Dekemper, E., Demoulin, P., Errera, Q., Franssens, G., Mateshvili, N., Pereira, N., Pieroux, D., and Vanhellemont, F.: The ALTIUS atmospheric limb sounder, J. Quant. Spectrosc. Ra., 238, 106542, https://doi.org/10.1016/j.jqsrt.2019.06.021, 2019.

Herman, B. M., Ben-David, A., and Thome, K. J.: Numerical technique for solving the radiative transfer equation for a spherical shell atmosphere, Appl. Optics, 33, 1760–1770, https://doi.org/10.1364/AO.33.001760, 1994.

Herman, B. M., Caudill, T. R., Flittner, D. E., Thome, K. J., and Ben-David, A.: Comparison of the Gauss–Seidel spherical polarized radiative transfer code with other radiative transfer codes, Appl. Optics, 34, 4563–4572, https://doi.org/10.1364/AO.34.004563, 1995.

Hovenier, J. W., Mee, van der Mee, C. V. M., and Domke, H.: Transfer of Polarized Light in Planetary Atmospheres: Basic Concepts and Practical Methods, Astrophysics and Space Science Library, Springer, the Netherlands, https://doi.org/10.1007/978-1-4020-2856-4, 2004.

Kokhanovsky, A. A., Budak, V. P., Cornet, C., Duan, M., Emde, C., Katsev, I. L., Klyukov, D. A., Korkin, S. V., C-Labonnote, L., Mayer, B., Min, Q., Nakajima, T., Ota, Y., Prikhach, A. S., Rozanov, V. V., Yokota, T., and Zege, E. P.: Benchmark results in vector atmospheric radiative transfer, J. Quant. Spectrosc. Ra., 111, 1931–1946, https://doi.org/10.1016/j.jqsrt.2010.03.005, 2010.

Korkin, S., Yang, E.-S., Spurr, R., Emde, C., Krotkov, N., Vasilkov, A., Haffner, D., Mok, J., and Lyapustin, A.: Revised and extended benchmark results for Rayleigh scattering of sunlight in spherical atmospheres, J. Quant. Spectrosc. Ra., 254, 107181, https://doi.org/10.1016/j.jqsrt.2020.107181, 2020.

Kozun, M., Bourassa, A., Degenstein, D., and Loewen, P.: A multi-spectral polarimetric imager for atmospheric profiling of aerosol and thin cloud: Prototype design and sub-orbital performance, Rev. Sci. Instrum., 91, 103106, https://doi.org/10.1063/5.0016129, 2020.

Kyrölä, E., Tamminen, J., Leppelmeier, G. W., Sofieva, V., Hassinen, S., Bertaux, J. L., Hauchecorne, A., Dalaudier, F., Cot, C., Korablev, O., Fanton d'Andon, O., Barrot, G., Mangin, A., Théodore, B., Guirlet, M., Etanchaud, F., Snoeij, P., Koopman, R., Saavedra, L., Fraisse, R., Fussen, D., and Vanhellemont, F.: GOMOS on Envisat: An overview, Adv. Space Res., 33, 1020–1028, https://doi.org/10.1016/S0273-1177(03)00590-8, 2004.

Llewellyn, E. J., Lloyd, N. D., Degenstein, D. A., Gattinger, R. L., Petalina, S. V., Bourassa, A. E., Wiensz, J. T., Ivanov, E. V., McDade, I. C., Solheim, B. H., McConnell, J. C., Haley, C. S., Savigny, C. v., Sioris, C. E., McLinden, C. A., Griffioen, E., Kaminski, J., Evans, W. F. J., Puckrin, E., Strong, K., Wehrle, V., Hum, R. H., Kendall, D. J. W., Matsushita, J., Murtagh, D. P., Brohede, S., Stegman, J., Witt, G., Barnes, G., Payne, W. F., Piche, L., Smith, K., Warshaw, G., Deslauniers, D. L., Marchand, P., Richardson, E. H., King, R. A., Wevers, I., McCreath, W., Kyrölä, E., Oikarinen, L., Leppelmeier, G. W., Auvinen, H., Megle, G., Hauchecorne, A., Lefevre, F., de La Noe, J., Ricaud, P., Frisk, U., Sjoberg, F., Scheele, F. v., and Nordh, L.: The OSIRIS instrument on the Odin spacecraft, Can. J. Phys., 82, 411–422, 2004.

Loughman, R., Flittner, D., Nyaku, E., and Bhartia, P. K.: Gauss–Seidel limb scattering (GSLS) radiative transfer model development in support of the Ozone Mapping and Profiler Suite

(OMPS) limb profiler mission, Atmos. Chem. Phys., 15, 3007–3020, https://doi.org/10.5194/acp-15-3007-2015, 2015.

Loughman, R. P., Griffioen, E., Oikarinen, L., Postylyakov, O. V., Rozanov, A., Flittner, D. E., and Rault, D. F.: Comparison of radiative transfer models for limb-viewing scattered sunlight measurements, J. Geophys. Res.-Atmos., 109, D06303, https://doi.org/10.1029/2003JD003854, 2004.

Loughman, R. P., Flittner, D. E., Herman, B. M., Bhartia, P. K., Hilsenrath, E., and McPeters, R. D.: Description and sensitivity analysis of a limb scattering ozone retrieval algorithm, J. Geophys. Res., 110, D19301, https://doi.org/10.1029/2004JD005429, 2005.

Malicet, J., Daumont, D., Charbonnier, J., Parisse, C., Chakir, A., and Brion, J.: Ozone UV spectroscopy. II. Absorption cross-sections and temperature dependence, J. Atmos. Chem., 21, 263–273, 1995.

Malinina, E., Rozanov, A., Rozanov, V., Liebing, P., Bovensmann, H., and Burrows, J. P.: Aerosol particle size distribution in the stratosphere retrieved from SCIAMACHY limb measurements, Atmos. Meas. Tech., 11, 2085–2100, https://doi.org/10.5194/amt-11-2085-2018, 2018.

Malinina, E., Rozanov, A., Rieger, L., Bourassa, A., Bovensmann, H., Burrows, J. P., and Degenstein, D.: Stratospheric aerosol characteristics from space-borne observations: extinction coefficient and Ångström exponent, Atmos. Meas. Tech., 12, 3485–3502, https://doi.org/10.5194/amt-12-3485-2019, 2019.

Malinina, E., Rozanov, A., Niemeier, U., Peglow, S., Arosio, C., Wrana, F., Timmreck, C., von Savigny, C., and Burrows, J. P.: Changes in stratospheric aerosol extinction coefficient after the 2018 Ambae eruption as seen by OMPS-LP and ECHAM5-HAM, Atmos. Chem. Phys. Discuss. [preprint], https://doi.org/10.5194/acp-2020-749, in review, 2020.

Marchuk, G. I., Mikhailov, G. A., Nazareliev, M., Darbinjan, R. A., Kargin, B. A., and Elepov, B. S.: The Monte Carlo methods in atmospheric optics, vol. 12, Springer-Verlag Berlin Heidelberg, available at: https://www.springer.com/gp/book/9783662135037 (last access: 22 May 2021), 2013.

Mauldin, L. E., Salikhov, R., Habib, S., Vladimirov, A. G., Carraway, D., Petrenko, G., and Comella, J.: Meteor-3M(1)/Stratospheric Aerosol and Gas Experiment III (SAGE III) jointly sponsored by the National Aeronautics and Space Administration and the Russian Space Agency, Proc. SPIE 3501, Optical Remote Sensing of the Atmosphere and Clouds, https://doi.org/10.1117/12.317767, 1998.

Mayer, B.: Radiative transfer in the cloudy atmosphere, EPJ Web of Conferences, 1, 75–99, https://doi.org/10.1140/epjconf/e2009-00912-1, 2009.

Mayer, B. and Kylling, A.: Technical note: The libRadtran software package for radiative transfer calculations – description and examples of use, Atmos. Chem. Phys., 5, 1855–1877, https://doi.org/10.5194/acp-5-1855-2005, 2005.

McLinden, C. A. and Bourassa, A. E.: A Systematic Error in Plane-Parallel Radiative Transfer Calculations, J. Atmos. Sci., 67, 1695–1699, https://doi.org/10.1175/2009JAS3322.1, 2010.

McLinden, C. A., Haley, C. S., Lloyd, N. D., Hendrick, F., Rozanov, A., Sinnhuber, B.-M., Goutail, F., Degenstein, D. A., Llewellyn, E. J., Sioris, C. E., Roozendael, M. V., Pommereau, J. P., Lotz, W., and Burrows, J. P.: Odin/OSIRIS observations of stratospheric BrO: Retrieval methodology, climatology, and inferred Bry, J. Geophys. Res.-Atmos., 115, D15308, https://doi.org/10.1029/2009JD012488, 2010.

Mishchenko, M. I., Lacis, A. A., and Travis, L. D.: Errors induced by the neglect of polarization in radiance calculations for rayleigh-scattering atmospheres, J. Quant. Spectrosc. Ra., 51, 491–510, https://doi.org/10.1016/0022-4073(94)90149-X, 1994.

Murtagh, D., Frisk, U., Merino, F., Ridal, M., Jonsson, A., Stegman, J., Witt, G., Jiménez, C., Megie, G., Noë, J. D., Ricaud, P., Baron, P., Pardo, J. R., Llewellyn, E. J., Degenstein, D. A., Gattinger, R. L., Lloyd, N. D., Evans, W. F. J., McDade, I. C., Haley, C. S., Sioris, C. E., Savigny, V., Solheim, B. H., McConnell, J. C., Richardson, E. H., Leppelmeier, G. W., Auvinen, H., and Oikarinen, L.: An overview of the Odin atmospheric mission, Can. J. Phys., 80, 309–318, https://doi.org/10.1139/P01-157, 2002.

Natraj, V. and Hovenier, J.: Polarized light reflected and transmitted by thick Rayleigh scattering atmospheres, Astrophys. J., 748, 28, https://doi.org/10.1088/0004-637X/748/1/28, 2012.

Oikarinen, L.: Polarization of light in UV-visible limb radiance measurements, J. Geophys. Res.-Atmos., 106, 1533–1544, https://doi.org/10.1029/2000JD900442, 2001.

Oikarinen, L.: Effect of surface albedo variations on UV-visible limb-scattering measurements of the atmosphere, J. Geophys. Res.-Atmos., 107, ACH 13-1–ACH 13-15, https://doi.org/10.1029/2001JD001492, 2002.

Oikarinen, L., Sihvola, E., and Kyrölä, E.: Multiple scattering radiance in limb-viewing geometry, J. Geophys. Res., 104, 31261–31274, https://doi.org/10.1029/1999JD900969, 1999.

Palmer, K. F. and Williams, D.: Optical Constants of Sulfuric Acid; Application to the Clouds of Venus?, Appl. Optics, 14, 208–219, https://doi.org/10.1364/AO.14.000208, 1975.

Postylyakov, O.: Linearized vector radiative transfer model MCC++ for a spherical atmosphere, J. Quant. Spectrosc. Ra., 88, 297–317, https://doi.org/10.1016/j.jqsrt.2004.01.009, 2004.

Ramon, D., Steinmetz, F., Jolivet, D., Compiègne, M., and Frouin, R.: Modeling polarized radiative transfer in the ocean-atmosphere system with the GPU-accelerated SMART-G Monte Carlo code, J. Quant. Spectrosc. Ra., 222–223, 89–107, https://doi.org/10.1016/j.jqsrt.2018.10.017, 2019.

Rault, D. F.: Ozone profile retrieval from Stratospheric Aerosol and Gas Experiment (SAGE III) limb scatter measurements, J. Geophys. Res., 110, D09309, https://doi.org/10.1029/2004JD004970, 2005.

Rault, D. F. and Loughman, R. P.: The OMPS Limb Profiler Environmental Data Record Algorithm Theoretical Basis Document and Expected Performance, IEEE Transactions on Geoscience and Remote Sensing, 51, 2505–2527, https://doi.org/10.1109/TGRS.2012.2213093, 2013.

Rault, D. F. and Spurr, R.: The OMPS Limb Profiler instrument: two-dimensional retrieval algorithm, Proc. SPIE, 7827, Remote Sensing of Clouds and the Atmosphere XV, 78270P, https://doi.org/10.1117/12.864799, 2010.

Rieger, L. A., Malinina, E. P., Rozanov, A. V., Burrows, J. P., Bourassa, A. E., and Degenstein, D. A.: A study of the approaches used to retrieve aerosol extinction, as applied to limb observations made by OSIRIS and SCIAMACHY, Atmos. Meas. Tech., 11, 3433–3445, https://doi.org/10.5194/amt-11-3433-2018, 2018.

Rieger, L. A., Zawada, D. J., Bourassa, A. E., and Degenstein, D. A.: A Multiwavelength Retrieval Approach for Improved

OSIRIS Aerosol Extinction Retrievals, J. Geophys. Res.-Atmos., 124, 7286–7307, https://doi.org/10.1029/2018JD029897, 2019.

Roth, C. Z., Degenstein, D. A., Bourassa, A. E., and Llewellyn, E. J.: The retrieval of vertical profiles of the ozone number density using Chappuis band absorption information and a multiplicative algebraic reconstruction technique, Can. J. Phys., 85, 1225–1243, https://doi.org/10.1139/p07-130, 2007.

Rozanov, A., Rozanov, V., and Burrows, J. P.: A numerical radiative transfer model for a spherical planetary atmosphere: combined differential–integral approach involving the Picard iterative approximation, J. Quantit. Spectrosc. Ra., 69, 491–512, https://doi.org/10.1016/S0022-4073(00)00100-X, 2001.

Rozanov, A., Eichmann, K.-U., von Savigny, C., Bovensmann, H., Burrows, J. P., von Bargen, A., Doicu, A., Hilgers, S., Godin-Beekmann, S., Leblanc, T., and McDermid, I. S.: Comparison of the inversion algorithms applied to the ozone vertical profile retrieval from SCIAMACHY limb measurements, Atmos. Chem. Phys., 7, 4763–4779, https://doi.org/10.5194/acp-7-4763-2007, 2007.

Rozanov, A., Kühl, S., Doicu, A., McLinden, C., Puķīte, J., Bovensmann, H., Burrows, J. P., Deutschmann, T., Dorf, M., Goutail, F., Grunow, K., Hendrick, F., von Hobe, M., Hrechanyy, S., Lichtenberg, G., Pfeilsticker, K., Pommereau, J. P., Van Roozendael, M., Stroh, F., and Wagner, T.: BrO vertical distributions from SCIAMACHY limb measurements: comparison of algorithms and retrieval results, Atmos. Meas. Tech., 4, 1319–1359, https://doi.org/10.5194/amt-4-1319-2011, 2011a.

Rozanov, A., Weigel, K., Bovensmann, H., Dhomse, S., Eichmann, K.-U., Kivi, R., Rozanov, V., Vömel, H., Weber, M., and Burrows, J. P.: Retrieval of water vapor vertical distributions in the upper troposphere and the lower stratosphere from SCIAMACHY limb measurements, Atmos. Meas. Tech., 4, 933–954, https://doi.org/10.5194/amt-4-933-2011, 2011b.

Rozanov, V., Rozanov, A., Kokhanovsky, A., and Burrows, J.: Radiative transfer through terrestrial atmosphere and ocean: Software package SCIATRAN, J. Quant. Spectrosc. Ra., 133, 13–71, https://doi.org/10.1016/J.JQSRT.2013.07.004, 2014.

Sioris, C. E., Rieger, L. A., Lloyd, N. D., Bourassa, A. E., Roth, C. Z., Degenstein, D. A., Camy-Peyret, C., Pfeilsticker, K., Berthet, G., Catoire, V., Goutail, F., Pommereau, J.-P., and McLinden, C. A.: Improved OSIRIS NO_2 retrieval algorithm: description and validation, Atmos. Meas. Tech., 10, 1155–1168, https://doi.org/10.5194/amt-10-1155-2017, 2017.

Taha, G., Rault, D. F., Loughman, R. P., Bourassa, A. E., and von Savigny, C.: SCIAMACHY stratospheric aerosol extinction profile retrieval using the OMPS/LP algorithm, Atmos. Meas. Tech., 4, 547–556, https://doi.org/10.5194/amt-4-547-2011, 2011.

Taha, G., Loughman, R., Zhu, T., Thomason, L., Kar, J., Rieger, L., and Bourassa, A.: OMPS LP Version 2.0 multi-wavelength aerosol extinction coefficient retrieval algorithm, Atmos. Meas. Tech., 14, 1015–1036, https://doi.org/10.5194/amt-14-1015-2021, 2021.

Thomason, L. W., Ernest, N., Millán, L., Rieger, L., Bourassa, A., Vernier, J.-P., Manney, G., Luo, B., Arfeuille, F., and Peter, T.: A global space-based stratospheric aerosol climatology: 1979–2016, Earth Syst. Sci. Data, 10, 469–492, https://doi.org/10.5194/essd-10-469-2018, 2018.

von Savigny, C., Ernst, F., Rozanov, A., Hommel, R., Eichmann, K.-U., Rozanov, V., Burrows, J. P., and Thomason, L. W.: Improved stratospheric aerosol extinction profiles from SCIAMACHY: validation and sample results, Atmos. Meas. Tech., 8, 5223–5235, https://doi.org/10.5194/amt-8-5223-2015, 2015.

Waters, J. W., Froidevaux, L., Harwood, R. S., Jarnot, R. F., Pickett, H. M., Read, W. G., Siegel, P. H., Cofield, R. E., Filipiak, M. J., Flower, D. A., Holden, J. R., Lau, G. K., Livesey, N. J., Manney, G. L., Pumphrey, H. C., Santee, M. L., Wu, D. L., Cuddy, D. T., Lay, R. R., Loo, M. S., Perun, V. S., Schwartz, M. J., Stek, P. C., Thurstans, R. P., Boyles, M. A., Chandra, K. M., Chavez, M. C., Chen, G. S., Chudasama, B. V., Dodge, R., Fuller, R. A., Girard, M. A., Jiang, J. H., Jiang, Y., Knosp, B. W., Labelle, R. C., Lam, J. C., Lee, K. A., Miller, D., Oswald, J. E., Patel, N. C., Pukala, D. M., Quintero, O., Scaff, D. M., Van Snyder, W., Tope, M. C., Wagner, P. A., and Walch, M. J.: The Earth Observing System Microwave Limb Sounder (EOS MLS) on the aura satellite, IEEE T. Geosci. Remote, 44, 1075–1092, https://doi.org/10.1109/TGRS.2006.873771, 2006.

Wiscombe, W. J.: Improved Mie scattering algorithms, Appl. Optics, 19, 1505–1509, 1980.

Zawada, D., Franssens, G., Loughman, R., Mikkonen, A., Rozanov, A., Emde, C., Bourassa, A., Dueck, S., Lindqvist, H., Ramon, D., Rozanov, V., Dekemper, E., Kyrölä, E., Burrows, J. P., Fussen, D., and Degenstein, D.: Radiance data for "Systematic Comparison of Vectorial Spherical Radiative Transfer Models in Limb Scattering Geometry" by Zawada et al., Zenodo, https://doi.org/10.5281/zenodo.4292303, 2020.

Zawada, D. J., Dueck, S. R., Rieger, L. A., Bourassa, A. E., Lloyd, N. D., and Degenstein, D. A.: High-resolution and Monte Carlo additions to the SASKTRAN radiative transfer model, Atmos. Meas. Tech., 8, 2609–2623, https://doi.org/10.5194/amt-8-2609-2015, 2015.

Zawada, D. J., Rieger, L. A., Bourassa, A. E., and Degenstein, D. A.: Tomographic retrievals of ozone with the OMPS Limb Profiler: algorithm description and preliminary results, Atmos. Meas. Tech., 11, 2375–2393, https://doi.org/10.5194/amt-11-2375-2018, 2018.